Particle Number Emission Indices from In-flight Aircraft

by

Steven Tran

A thesis submitted in partial fulfillment of the requirements for the degree of

Master of Science

Department of Mechanical Engineering
University of Alberta

Abstract

To reduce CO2 emissions, the aviation industry has begun looking into alternative biofuels as a replacement for conventional fossil-fuel based jet fuel. Although biofuels may reduce aircraft CO_2 emissions, it is also important to consider how other emissions are effected such as particle emissions. Aircraft particle emissions have been studied extensively in the lab or on the ground with stationary aircrafts or test engine cells with few studies measuring emissions from aircraft in-flight. To study in-flight particle emissions, the National Research Council of Canada has equipped a measurement aircraft with condensation particle counters and a catalytic denuder to measure both non-volatile and total (volatile and non-volatile) particles. Two separate flight campaigns were undertaken to collect emissions data from aircrafts in-flight.

The Civil Aviation Alternate Fuels Contrail and Emissions Research (CAAFCER) campaign involved the sampling of Air Canada Airbus A320 aircrafts during commercial flights. Two A320 aircraft equipped with CFM56-5A1 engines burning Jet A1 and a 43% hydrotreated esters and fatty acids (HEFA)/Jet A1 blend and another aircraft with CFM56-5B4/P engines burning Jet A1 were sampled. It was found that the particle number emission indices were similar amongst the tested engines and fuel types. The total particle emission index for particles greater than 7.7 nm ranged between 1.44×10^{17} to 2.17×10^{17} particles per kg of fuel, the total particle emission index for particles greater than 15.4 nm ranged between 1.73×10^{16} to 4.73×10^{16} kg^{-1}, and the non-volatile particle emission index for particles greater than 13.3 nm ranged from 3.55×10^{15} to 6.76×10^{15} kg^{-1}.

In the Civil Aviation Alternate Fuels Contrails and Emissions with high Blend Biojet (CAAFCEB) campaign, the Falcon 20 research aircraft was sampled in-flight while fueled with an ethanol-based (ATJ) biofuel, JP-5 fuel and Jet A1 fuel. The objective of this flight campaign

was to compare the particle emissions of the ATJ and JP-5 fuels to Jet A1 fuel. The total particle emissions for the JP-5 were found to be slightly larger than Jet A1 fuel with the total particle emissions for the JP-5 fuel being 1.29 to 1.52 times larger than for Jet A1. The ATJ biofuel on the other hand was found to significantly reduce total particle number emissions by up to 91% and non-volatile particle number emissions by 96% compared to Jet A1 fuel.

Preface

The experimental set-up, coordination of flights and collection of data was completed by the National Research Council of Canada in Ottawa. The analysis of the data and results presented in this work was completed by myself. The manuscript was completed by me with assistance from Dr. Olfert. Chapter 1 and 4 are my original work.

Chapter 2 of this thesis has been submitted for publication as S. Tran, M. Kazemimanesh, A. Brown, and J.S. Olfert, "Particle Number Emission Indices from In-Flight Commercial Aircraft", *Atmospheric Environment.*. I was responsible for the data analysis and manuscript composition. M. Kazemimanesh contributed with the particle loss model and manuscript edits. A. Brown was responsible for the data collection and assisted with manuscript edits. J.S. Olfert was the supervisory author and involved with the instrumentation set-up and manuscript composition.

Chapter 3 of this thesis will be submitted for publication as S. Tran, A. Brown, and J.S. Olfert, "Comparison of Particle Number Emissions from In-Flight Aircraft Fueled with Jet A1, JP-5 and Alcohol-to-Jet Fuel Mixturess", *Energy Fuels*. I was responsible for the data analysis and manuscript composition. A. Brown was responsible for the data collection and assisted with manuscript edits. J.S. Olfert was the supervisory author and involved with the instrumentation set-up and manuscript composition.

Acknowledgements

I would like to thank Dr. Olfert for providing me with this opportunity to pursue graduate studies and to be a part of this research project which allowed me to travel to Ottawa and work with the National Research Council of Canada. I am also grateful for all the help and ideas he provided throughout the duration of my studies.

I would also like to thank everyone at the National Research Council of Canada in Ottawa for all their help while I was at their facility as well as providing the data and helping me interpret all the data in order for me to complete my analysis.

Lastly, I would like to thank my friends and family for their continued support throughout the years. If it wasn't for them, I would not have been able to get to where I am today.

Table of Contents

List of Tables

List of Figures

Chapter 1 Introduction

The aviation sector is an important industry that supports over 65 million jobs worldwide and carried 4.1 billion passengers in 2017 (ATAG, 2018). It is an industry that is expected to continue growing with the possibility that the CO_2 emissions in 2050 may be three times that of 2005 (Lee, 2009). Even though airlines only contribute 2% of the global CO_2 anthropogenic emissions, an industry goal has been set to reduce CO_2 emissions to 50% of the 2005 levels by 2050 (ATAG, 2018). One way to reduce the net CO_2 emissions from aircrafts is to switch to biofuel as an alternative to conventional jet fuel (Wise et al., 2017). Moving away from petroleum-based sources of fuel and replacing them with more sustainable alternatives could result in an 80% reduction in CO2 emissions (ATAG, 2018). Although reducing CO_2 emissions from aircrafts is the main motivation for the interest in aviation biofuel, it is also important to understand the overall emission characteristics of a new fuel which include how biofuels affect particulate matter emissions.

1.1 What is particulate matter?

The World Health Organization defines particulate matter as a type of pollutant consisting of a mixture of liquid droplets and inhalable solid particles in the air (WHO, 2018). The major components of particulate matter include acids (such as sulphates and nitrates), black carbon (soot), and dust. Aircraft exhaust emissions contain both volatile and non-volatile particles (together referred to as total particles).

Volatile particles are particles that are formed by the nucleation of gas-phase components of the exhaust such as sulfur compounds which can form sulfuric acid (Anderson B. E. et al.,

1998; Schröder et al., 2000). Organic carbon is also a volatile component that may be present on soot as a coating on the individual spherical particles (Petzold et al., 2013). The "volatility" of the particulate matter is defined operationally. Non-volatile material is often defined as material that does not evaporate after heating the sample to a temperature in the range of 300 to 400 ^{o}C. (SAE, 2018, 2006).

Non-volatile particles found in aircraft exhaust generally consists of soot (Stacey, 2019). Soot particles are formed from agglomerates of spherical carbonaceous particles composed of graphite-like microstructures and are comprised mostly of carbon with minor amounts of hydrogen and oxygen (Petzold et al., 2013). Figure 1(a) shows images of soot particles taken with high-resolution transmission electron microscopy. In Figure 1(a), the first row shows the soot particle agglomerates while the second row shows the primary spherical particles and the last row shows the microstructure where the graphite layers are visible.

Soot particles from aircraft jet engines are typically in the range of 20-50 nm (Anderson, 2011; Chan et al., 2015; Corporan et al., 2007; Lopes et al., 2019; Schröder et al., 2000; Stacey, 2019; Vander Wal et al., 2014). Figure 1(b) shows an example of the geometric mean size distributions for both total and non-volatile particles measured from aircraft exhaust emissions in flight at cruise conditions by Moore et al. (2017). In this example, the geometric mean diameter of both total and non-volatile particles is around 30 nm.

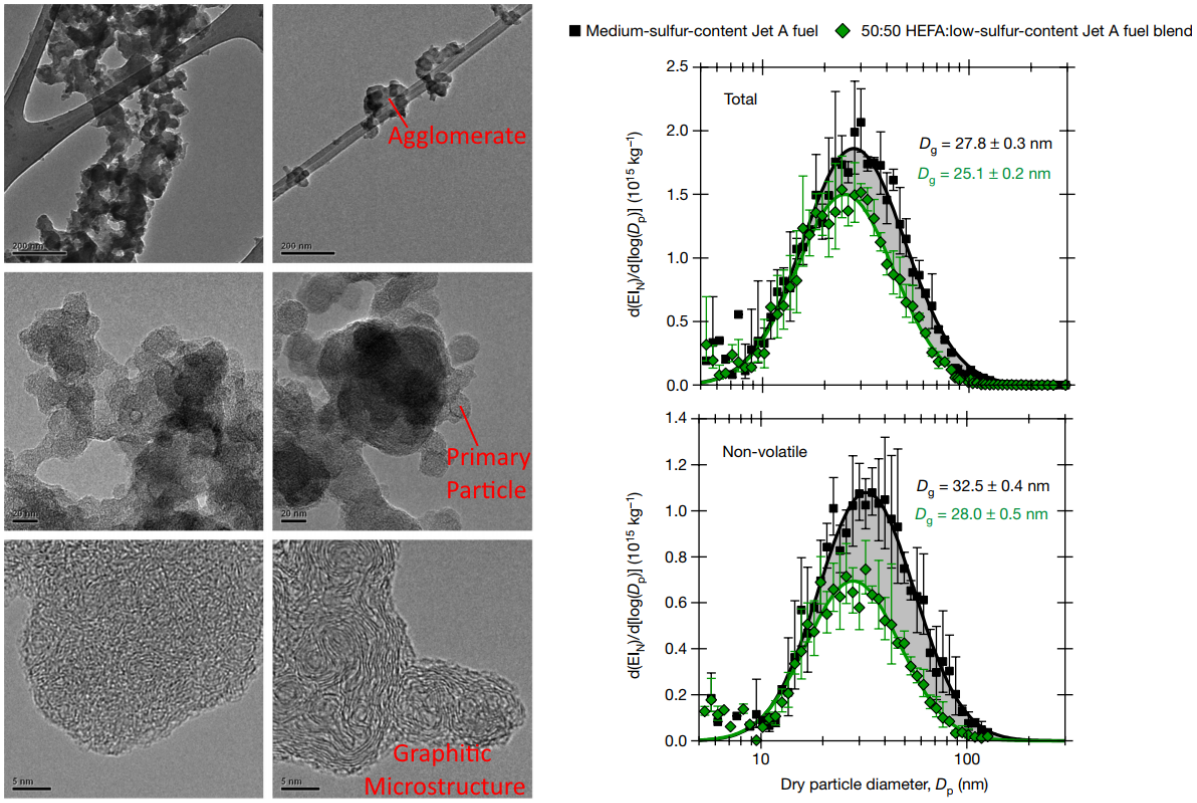

Figure 1. (a) HRTEM images (from low to high magnification) of derived soot macro- micro- and nano-structure; left column images show particles from low (4-7%) engine power and the right column shows particles from high (100%) engine power (Vander Wal et al., 2014) (b) Geometric mean size distributions of particle emissions at high-thrust and cruise conditions (Moore et al., 2017).

1.2 Environmental and health effects

Aircrafts are generally powered by engines which burn fossil fuels releasing a variety of emissions as a byproduct. A unique problem with aircraft emissions is that a large portion of the emissions are emitted at altitude during flight. This leads to concerns regarding their environmental and health impacts both in the air and at ground level.

1.2.1 Environmental effects

The most visible impact aviation has on the environment are the formation of contrails. In the atmosphere, particulate matter emitted from aircraft engines can act as cloud condensation nuclei leading to contrail formation which could contribute to cirrus cloud formation (Lee, 2009). Contrails form when water condenses onto the particles which immediately freeze. The particles continue to grow as water vapor in the atmosphere deposit on the frozen particles (Lee, 2009). The formation of contrails is dependent on the ambient atmospheric conditions as 98% of the water mass of contrails originates from the atmosphere (Lee, 2009).

Radiative forcing is a measure of how the energy balance of the Earth-atmosphere system is affected by factors such as greenhouse gases, aerosol and clouds in the atmosphere (He et al., 2018; Pulselli and Marchi, 2015). Radiative forcing is often used to quantify how various factors contribute to climate change as they change the balance between incoming solar radiation and outgoing infrared radiation within the atmosphere (He et al., 2018; Pulselli and Marchi, 2015).

Contrails in the atmosphere have a cooling effect on the Earth by reflecting solar radiation back into space and a warming effect by reducing the amount of radiation leaving the earth. Despite these contradicting effects, aircraft-induced contrails are estimated to have a net warming effect (Lee, 2009). Although there are large uncertainties in the estimates of the radiative forcing of aircraft-induced contrails, the minimum range is estimated to be around 5-10 $mW \cdot m^{-2}$ (Lee, 2009). In comparison, the global average radiative forcing of CO_2 is approximately 2 $W \cdot m^{-2}$ (US Department of Commerce, 2020) which is much larger in comparison to that of contrails but with the growing aviation industry, the estimated effect of contrails may also continue to grow.

1.2.2 Health effects

Barrett et al. (2010) conducted a study that indicated that aircraft cruise emissions can cause premature mortality and should be considered when evaluating aircraft emissions. A study with mice showed that aircraft particle emission exposure resembles that of diesel exhaust which has been linked to lung cancer (Bendtsen et al., 2019). Examination of histological lung sections showed remnants of particles after 28 and 90 days of exposure to airport particles. An increase in inflammation and DNA damage was also observed. The particles collected at the airport were small (diameters of 10-30 nm) and it was predicted that 9.6% of the particles exposed to the airfield personnel would deposit in the alveolar region of the lungs.

It has also been shown that bronchial epithelial cells exposed to non-volatile particles from jet engines increases cell membrane damage, leads to oxidative stress and affects the pro-inflammatory response (Jonsdottir et al., 2019). Additionally, the amount of impact the non-volatile particles have on the bronchial epithelial cells may also be affected by the engine thrust level and type of fuel used. At ground idle power, the cytotoxicity of non-volatile particles from Jet A1 fuel was significantly higher than for a 32% hydro-processed esters and fatty acid (HEFA) blend. On the other hand, at 85% thrust, non-volatile particles from the HEFA blend had a higher level of cytotoxicity.

In addition to adverse effects of particles on the respiratory system, the small particles found in aircraft exhaust also has the potential to translocate into the blood circulation which would affect cardiovascular health (Terzano et al., 2010). Due to their size, the particles can rapidly move from the lungs and into the blood which would distribute the particles throughout the body. This could potentially further affect other organs such as the liver, the kidneys, the heart and the brain where particles may deposit.

1.3 Particulate matter regulation

To control and regulate emissions, aircraft engines are required to meet emissions certifications outlined in the International Civil Aviation Organization (ICAO) Annex 16 Volume II Aircraft Engine Emissions (2017) which were designed in response to concerns about the environmental impacts of aviation industry. The standard outlines specific procedures and test conditions that must be met when testing turbojet and turbofan emissions. Currently regulated aircraft emissions are smoke and gaseous emissions which include unburned hydrocarbons (HC), carbon monoxide (CO) and oxides of nitrogen (NO_x). The emission measurements are required to be taken at the reference operating conditions defined in the landing and take-off (LTO) cycle outlined in Table 1.

Table 1. LTO cycle as defined in the ICAO Annex 16 standard.

LTO	Thrust Setting (% of rated thrust)
Take-off	100
Climb	85
Approach	30
Taxi/ground idle	7

Currently, the only particle emission regulated is black carbon (soot) through sampling the exhaust smoke and evaluated by the smoke number (SN). In addition to the ICAO certification standards, the Society of Automotive Engineers (SAE) has similar regulations regarding aircraft engine exhaust smoke outlined in ARP1179 (SAE, 1970). The smoke number is a dimensionless term that quantifies smoke emissions based on the relative reflectance of the soot collected on a filter. The smoke number for individual samples (SN') is calculated by:

$$SN' = 100\left(1 - \frac{R_s}{R_w}\right) \quad (1)$$

where R_s is the absolute reflectance of the stained filter and R_w is the absolute reflectance of a clean filter. Although an algorithm has been developed that correlates smoke number with the black carbon mass emission index (Peck et al., 2013), the smoke number does not provide any details on the size or number of particles emitted. Therefore, a large number of smaller particles could have the same mass collected on a filter as a smaller number of larger particles which would result in similar smoke number values.

Recently, ICAO has amended the ICAO Annex 16 Volume II (2017) standard for aircraft engine emissions with a new addition which provides recommendations for the assessment of non-volatile particulate matter. This addition was a result of the Tenth meeting of the Committee on Aviation Environmental Protection (CAEP/10) which was held in February 2016 at the ICAO headquarters (ICAO, 2016). The new non-volatile particulate matter standards will apply to in-production engines with a rated thrust greater than 26.7 kN by January 1 2020 or later. Although a new standard for non-volatile particulate matter has been adopted, it does not introduce a new stringency compared to the existing exhaust smoke standard with the smoke number. That is, any engine that passes the current smoke number standard will also pass the new non-volatile particulate matter standard. This is by design as the new non-volatile particulate matter standard is based on a mass concentration limit that is equivalent to the SN regulatory levels. As such, this is just the first step towards developing more stringent standards related to aircraft emissions particles. The new non-volatile particulate matter standard now requires manufacturers to report the non-volatile particulate matter mass and number emission indices at each of the point of the LTO cycle as well as the maximum non-volatile particulate matter mass emission index, maximum non-volatile particulate matter number emission index and maximum non-volatile particulate matter mass concentration. Similarly, the SAE released a new standard related to the

continuous sampling and measurement of non-volatile particulate matter emissions from aircraft engines in the ARP6320 standard (SAE, 2018). The standard specifies that the particle number concentration must be measured by an instrument with a cut-off diameter of 10 nm.

In order for the CAEP to develop a non-volatile particulate matter mass and number standard, they require data from 25 in-production and project engines that are representative of the current and future aircraft fleet (ICAO, 2016). This data will be used to develop LTO-based non-volatile particulate matter mass and number metric systems, stringency options, technology response and cost effectiveness analysis. There are also plans to develop corrections for non-volatile particulate matter emissions to take into account ambient conditions and fuel sensitivity. Additionally, new maximum non-volatile particulate matter mass concentration data will be used along with the smoke number emissions data to update the mass concentration-smoke number relationship which could lead to the replacement of the smoke number system with a maximum non-volatile particulate matter mass concentration. It is important to note that current regulations only deal with non-volatile particles.

1.4 Aviation fuels

Gas turbine engines are typically fueled by kerosene-type fuels (Lois et al., 2003). For civil commercial aircrafts, Jet A1 or Jet A are most commonly used while JP-8 is the main fuel used in military aviation (Lois et al., 2003). The ASTM D1655-19 standard provides requirements for aviation turbine fuels (Jet A/A1) derived from conventional sources such as crude oil, natural gas liquid condensates, heavy oil, shale oil and oil sands. Since the exact composition of Jet A/A1 fuel is difficult to control, the ASTM standard has evolved as a performance specification. With respect to the composition of Jet A/A1 fuels, the standard

specifies the maximum fuel aromatic content allowed is 26.5% by volume while the maximum fuel sulfur content allowed is 3000 ppm. The difference between Jet A and Jet A1 fuels are the freezing points which are -40°C and -47°C respectively. JP-8 fuel is the military equivalent of Jet A1 but with additional additives such as anti-icing additive, corrosion inhibitor and antistatic additive (Lois et al., 2003). JP-5 is an older iteration of jet fuel that is still used today by the U.S. Naval air force with a higher flash point (60°C compared to a minimum of 38°C for Jet A/A1 and JP-8) and no antistatic additives (Lois et al., 2003).

ASTM has approved of a number of alternative jet fuels that can be blended up to 50% by volume with conventional jet fuel specified in the ASTM D7566-19 standard. This includes both hydro-processed esters and fatty acids (HEFA) fuel and alcohol-to-jet (ATJ) fuel. HEFA fuel is produced from a hydroprocessing pathway which involves the chemical conversion of triglyceride feedstock (such as vegetable oil, animal fat and used cooking oil) to produce a biojet fuel (Gutiérrez-Antonio et al., 2017). The triglyceride feedstock goes through hydrodeoxygenation, hydroisomerizing and hydrocracking which results in a number of products where the biojet fuel is separated through distillation (Gutiérrez-Antonio et al., 2017). A block diagram is shown in Figure 2. HEFA biofuel differs from conventional Jet A/A1 fuel by being relatively free of aromatic and sulfur content (Kandaramath Hari et al., 2015; Vozka et al., 2018). It has also been shown that the source of feedstock can also affect the final biojet fuel properties; for example, a study Vozka et al. (2018) comparing HEFA biojet fuel composition to Jet A found that biojet fuel processed from mixed fat had a higher freezing point than biojet fuel made from camelina or tallow and Jet A fuel. They also found that the flash point value of HEFA biojet fuel made from camelina and mixed fats was lower than Jet A (Vozka et al., 2018).

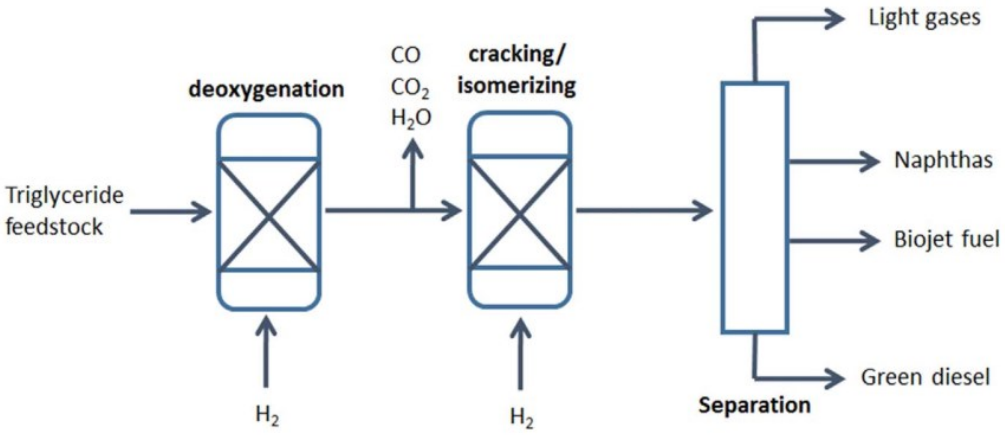

Figure 2. Block diagram of hydroprocessing pathway to convert triglyceride feedstock into biojet fuel (Gutiérrez-Antonio et al., 2017).

For the alcohol-to-jet pathway, sugar and starchy feedstock is first converted into alcohols through fermentation (Gutiérrez-Antonio et al., 2017). The alcohols are then converted into a biojet fuel through dehydration, oligomerization and hydrogenation (Gutiérrez-Antonio et al., 2017) although current standards only allow ATJ biofuels derived from ethanol or isobutanol (ASTM D7566-19, 2019). A block diagram for the ATJ pathway is shown in Figure 3. Similar to the HEFA biofuel, ATJ biofuel does not contain any aromatic and sulfur content (Schripp et al., 2019). The ATJ pathway is not as developed as the HEFA pathway, thus it is currently not as widely used resulting in less available information on ATJ biojet fuels.

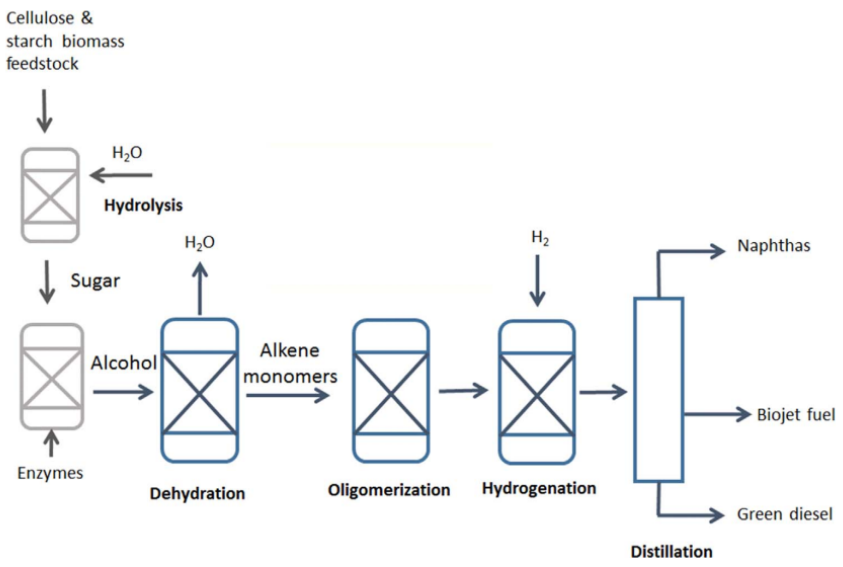

Figure 3. Block diagram of alcohol-to-jet pathway to convert sugar and starchy feedstock into biojet fuel (Gutiérrez-Antonio et al., 2017).

1.5 Previous studies on aircraft particulate matter

Numerous studies have been undertaken to better understand the effect of fuel type and composition on aircraft emissions through ground tests and in-flight measurements. A number of lab tests have been completed which showed that alternative biofuels such as Fischer-Tropsch can reduce particle number emissions compared to conventional jet fuel (Corporan et al., 2007; DeWitt et al., 2008; Corporan et al., 2011; Lobo et al., 2011).

1.5.1 Laboratory and ground-based tests

1.5.1.1 Fuel aromatic content and non-volatile particles

Corporan et al. (2007) conducted a study comparing non-volatile particle emissions from burning a petroleum-based JP-8 jet fuel and Fischer-Tropsch fuel blends of 25% to 100% in a T63-A-700 turboshaft engine and an atmospheric swirl-stabilized research combustor. They found that the non-volatile particle emissions decreased with increasing concentration of Fischer-

Tropsch fuel with a reduction of over 70% in particle numbers measured from the 100% Fischer-Tropsch blend to JP-8 at cruise power. The decrease in particle numbers is likely due to the reduced amount of aromatic content in the Fischer-Tropsch fuel and blends compared to the JP-8 fuel. The higher hydrogen-to-carbon content in the Fischer-Tropsch fuel is also thought to have contributed to the reduction in soot. On the other hand, the Fischer-Tropsch fuel had a negligible effect on gaseous emissions.

Using a similar set-up with a T63-A-700 turboshaft engine, DeWitt et al. (2008) conducted lab tests to compare emissions from Fischer-Tropsch fuel with varying concentrations of aromatic content to conventional JP-8 jet fuel. They found that non-volatile particle number emissions increased with increasing aromatic content and the JP-8 fuel produced 4.5 times more particles than neat Fischer-Tropsch fuel. The aromatic content in jet fuel is also believed to provide seal-swell among other "fit-for-purpose" properties required for jet fuels. Therefore, the neat Fischer-Tropsch fuel's lack of aromatic content means that Fischer-Tropsch fuel would require additional additives to meet those requirements. Although the addition of aromatic content to Fischer-Tropsch fuel would increase the particle number emissions, they showed that it is possible to achieve similar seal swelling to that of JP-8 fuel while still reducing particle emissions.

Another study by Corporan et al. (2011) using the same experimental set-up with a T63-A-700 turboshaft engine evaluated six different alternative jet fuels compared to conventional JP-8 jet fuel; three alternative fuels were produced through a Fischer-Tropsch process and the other three were produced through hydro-processing. The study found that the use of alternative fuels significantly reduced emissions by 90-98% at idle and 60-80% at cruise which agree with

previous findings. Again, the reduction in particle emissions was likely due to the alternative fuels being mostly aromatic-free. The lack of aromatic content in the alternative fuels also resulted in reduced volume swell of O-rings compared to JP-8 fuel. On the other hand, the amount of volume swell was still significant because aromatic content is not the only factor that influences the swelling of O-rings. Fuel composition such as the molecular weight distribution and the type of material of the O-rings also affect the amount of volume swell.

Lobo et al. (2011) tested conventional Jet A1 jet fuel, varying blends of Jet A1 with an alternative biomass-based (fatty acid methyl ester, FAME) (20% and 40% FAME blends), 100% Fischer-Tropsch -based fuel and a 50/50 Fischer-Tropsch fuel blend with a CFM56-7B commercial jet engine. Total particle emissions were measured. Consistent with previous studies, Lobo et al. (2011) found that the particle number emissions decreased with decreasing fuel aromatic content with the largest reduction of 52% with the 100% Fischer-Tropsch fuel compared to Jet A1. It was also found that the geometric mean diameters (GMD) of the particle emissions decreased with increasing alternative fuel blends and the 100% Fischer-Tropsch fuel produced the smallest GMD.

Timko et al. (2010) conducted comprehensive tests on a Pratt & Whitney PW308 gas turbine engine burning three types of fuel: conventional JP-8 fuel, a “zero sulfur” and “zero aromatic” Fischer-Tropsch fuel made from natural gas feedstock and a 50/50 blend of the JP-8 and Fischer-Tropsch fuel. Similar findings were reported where switching to the Fischer-Tropsch fuel reduced non-volatile particle number emissions and were most prominent at idle where the non-volatile particle numbers for Fischer-Tropsch fuel were only 9% of those measured for JP-8. The 50/50 blend also reduced non-volatile particle emissions, but the reduction was not

proportional to the volume blended (at idle, the 50/50 blend non-volatile particle numbers were 59% of the JP-8 fuel). The 50/50 blend also appeared to increase non-volatile particle emissions by 3%. With the primary difference between the JP-8 and Fischer-Tropsch fuel being the aromatic content, the findings support previous studies which correlate fuel aromatic content and soot emissions. They also found that the impact of fuel properties on non-volatile particle number emissions decreased with increasing power.

NASA has also conducted tests on alternative fuels in the Alternative Aviation Fuel Experiment (AAFEX-I) (Anderson, 2011; Beyersdorf et al., 2014). Five different fuels were tested: JP-8, natural gas-based Fischer-Tropsch fuel, coal-based Fischer-Tropsch fuel and 50/50 blends of the two Fischer-Tropsch fuels with JP-8. The test aircraft was a DC-8 test with four CFM-56-2C1 engines which was parked on tarmac with exhaust inlet probes located 1, 30 and 145 m behind the two inner engines. They found that the natural gas-based Fischer-Tropsch fuel provided the greatest non-volatile particle number reductions; at idle (4% of maximum thrust), the particle numbers were 200 times lower than JP-8 and as power increased, the relative reduction in emissions decreased so at 85% of maximum thrust, particle emissions were only about 4 times lower than JP-8. The coal-based Fischer-Tropsch fuel provided slightly lower emission reductions with a 20 times reduction in particle numbers at idle and peaking at medium-thrust levels with a 50 times reduction compared to JP-8. The emission reduction at 85% was the same for both neat Fischer-Tropsch fuels.

Brem et al. (2015) performed lab experiments to specifically test the effects of fuel aromatic content on non-volatile particle emissions. No alternative fuel was used in these experiments; instead neat Jet A1 fuel with an aromatic content of 17.8% (v/v) was injected with

two aromatic solvents to increase the fuel aromatic content of up to 23.6% (v/v). One solvent contained 6% (v/v) naphthalenes while the other solvent did not contain any. As expected, the higher aromatic content resulted in increased soot formation. Non-volatile particle numbers increased by a factor of 1.51 for an increase of 5.8% (v/v) in fuel aromatic content at 30% thrust. At 100% thrust the effect of fuel aromatic content decreased as non-volatile particle numbers only increased by a factor of 1.06 which is in line with the findings by Timko et al. (2010). In addition to the amount of aromatic content and power setting, the type of aromatic content also affects non-volatile particles. Switching from monoaromatics to naphthalenes from 0.78% (v/v) to up to 1.19% (v/v) at similar aromatic content levels resulted in up to 30% higher non-volatile particle numbers at 30% thrust. The dependence of soot formation on aromatic content is explained as aromatic molecules act as condensation and addition sites for the products of incomplete combustion which form polycyclic aromatic hydrocarbons that nucleate and carbonize to form soot.

1.5.1.2 Volatile particles

During NASA's AAFEX-I experiments, inlet probes were positioned at various distances behind the engines and the effect of age on particle emissions was also observed (Anderson, 2011; Beyersdorf et al., 2014). At the exhaust plane of the engine, only soot-mode particles were measured while additional nucleation-mode particles were measured downwind. The largest increase in total particle numbers was observed between 1 and 30 m with two orders of magnitude increase in particle numbers at low power settings and about an order of magnitude increase at high power settings. Between 30 to 145 m, total particle numbers increased slightly with an increase of up to 50% observed. The nucleation of volatile particles is largely affected by the ambient temperature with a decrease in nucleation seen as ambient temperature increases.

The temperature dependence also seems to be stronger at low power and is relatively constant at higher powers. Despite the formation of volatile particles for all fuels, the neat Fischer-Tropsch fuels still provided a significant reduction in total particles (between 1-2 orders of magnitude decrease). Similarly, Timko et al. (2010) also found that the Fischer-Tropsch fuel exhaust plumes did not contain any nucleation/growth mode particles as opposed to the JP-8 and 50/50 blend duels. This is likely due to the lack of fuel sulfur content in the neat Fischer-Tropsch fuel.

Lab and ground-based experiments do not generally measure volatile particles because, as seen from AAFEX-I, they require time to form and grow. Thus, the effect of fuel sulfur content (FSC) on aircraft particle emissions is better examined from in-flight experiments where exhaust plumes from source aircrafts are sampled in the air by research aircrafts. Since these reactions also depend on temperature, pressure, local fuel-to-air equivalence ratio and residence time, this helps to explain why the operating power of the engine affects particle emissions.

1.5.2 In-flight measurements

The laboratory and ground tests provide some information for characterizing aircraft emissions and how emissions are affected by fuel composition. Unfortunately, most ground-based tests are not representative of the ambient conditions in the atmosphere at altitude where the majority of aircrafts spend their time. For this reason, in-flight measurements of aircrafts are important for providing information on how emissions behave in their environment where they are most often emitted.

1.5.2.1 Fuel sulfur content

The effect of fuel sulfur content (FSC) on aircraft exhaust composition has been studied extensively through a series of experiments (Schumann et al., 2002). The first set of flights were

conducted during SULFUR 2 (Schumann et al., 1996) with contrails generated by the ATTAS (Advanced Technologies Testing Aircraft System) of DLR (German Aerospace Center) while measurements were made with the Falcon research aircraft of DLR. The ATTAS was equipped with two Rolls Royce M45H Mk501 turbofan engines. The ATTAS engines are capable of being fueled by either the left- or right-wing tank; the left-wing tank contained Jet A1 fuel with a fuel sulfur content of 166 ppm while the right-wing tank contained Jet A1 fuel with a fuel sulfur content of 5400 ppm. They found that the increase in sulfur content caused a 25% increase in the number of particles larger than 7 nm and a 50% increase in the number of particles larger than 18 nm.

The second set of flights were completed during the SULFUR 5 (Schröder et al., 1998) campaign which again used the ATTAS as the source aircraft and the Falcon as the measurement aircraft. Similar to the SULFUR 2 campaign, a high sulfur fuel (2.7 g/kg fuel or 2700 ppm) and low sulfur fuel (0.02 g/kg fuel or 20 ppm) were used in the study and exhaust measurements were made in both contrail and non-contrail conditions. The results showed that non-volatile particle numbers are not dependent on the FSC of the fuel. Total particle numbers on the other hand were an order of magnitude higher for the high FSC fuel case compared to the low FSC fuel case. It was also found that the number of total particles larger than 5 nm was generally an order of magnitude higher than the number of total particles larger than 14 nm in no contrail conditions which means that a large number of total particles fall between the 5-14 nm range. Additionally, measurements of both non-volatile and total particle numbers were up to 2-4 times lower in contrail conditions compared to non-contrail conditions. This is likely due to the growth of ice particles rapidly decreasing the plume humidity and small liquid particles shrinking below

the detection limit of the particle counters as well as scavenging of smaller particles by larger ice particles.

The next campaign was completed during SULFUR 6 (Brock et al., 2000; Petzold et al., 1999; Schröder et al., 2000) which involved in-flight measurements behind the ATTAS research aircraft and a Boeing B737-300 burning fuel with low FSC (2.6 ppm) and high FSC (118 ppm for ATTAS and 56 ppm for B737). From total particle size distribution measurements made behind the B737, it was found that there was no significant shift in particle size for particles less than 10 nm in diameter between the two FSC cases (Brock et al., 2000) and most volatile particles were found in the <10 nm range (Schröder et al., 2000). The volatile particle numbers were found to increase with increasing plume age in non-contrail conditions while concentrations remained relatively constant in contrails (Schröder et al., 2000). Contrail conditions also reduced volatile particle numbers by an order of magnitude. Particles smaller than 5 nm detected at the low FSC case also suggests that other non-sulfate volatile particles condense in the exhaust plumes (Brock et al., 2000). It was also found that at low FSC values (~50-100 ppm) a large percent change in FSC did not significantly affect total particle numbers which may suggest that non-sulfate particles contribute a large fraction to volatile particle numbers at low FSC. Additionally, as expected the non-volatile particle numbers were found to be relatively constant across all FSC values (Petzold et al., 1999).

The most recent campaign was completed during SULFUR 7 with a focus on the effect of engine efficiency on contrail formation and emissions (Schumann et al., 2002). Two source aircrafts with differing engine efficiencies were used: an older Boeing B707 (with PW JT3D-3B model engine) and a modern Airbus A340 (with CFM56-5C4 model engines) with more efficient

engines. The results showed that in the young plumes at non-contrail conditions, the non-volatile particle numbers for the B707 were an order of magnitude higher than for the A340 with typical FSC values (120 and 380 ppm respectively). On the other hand, total particle numbers for particles larger than 5 nm for the A340 were about an order of magnitude higher than the B707 while total particle numbers for particles larger than 14 nm were comparable for the two aircrafts. Thus, although the older engines emit more non-volatile particles, the modern engines appeared to contribute a larger number of small ultrafine particles.

1.5.2.2 First biofuel flight measurements

As discussed previously, the effect of alternative biofuel on aircraft emissions has been tested extensively in a laboratory environment with promising results. The one issue is that most aircraft exhaust is emitted in the atmosphere where ambient conditions can differ and vary from those found in a lab. Therefore, it is important to also study the impacts of biofuels on emissions as they would occur in the atmosphere at altitude.

A series of flight experiments were conducted by NASA as a part of the Alternative Fuel Effects on Contrails and Cruise Emissions (ACCESS) campaign (Moore et al., 2017). Again the DC-8 was the source aircraft with the wing tanks fueled with a low (22 ppm)- or medium (416 ppm)-sulfur-content Jet A1 fuel while an auxiliary tank mounted on the fuselage was filled with a 50/50 blend of low-sulfur Jet A and a Camelina-based HEFA fuel. Instead of the DC-8 aircraft being parked on the ground, the measurements were done in flight at cruise conditions. The exhaust plumes were sampled by research aircrafts from NASA and, the German Aerospace Center (DLR) and the National Research of Council (NRC) Canada. Since the DC-8 aircraft has 4 engines which could be fueled separately by any of the fuel tanks, both fuels (either of the Jet

A1 and the HEFA blend) were burned simultaneously on each flight. This allowed for the measurements to be made for the fuels in the same atmospheric conditions. To avoid the mixing of the two plumes from the different engines and fuels, the research aircrafts trailed the source aircraft at a short distance (30-150 m). From the results, they found that the blending of petroleum-based fuel with a HEFA biofuel reduced both volatile and non-volatile particle number emissions by 50%-70%.

1.5.3 Summary of previous studies

In summary, several factors were found to affect particle number emissions in aircraft emissions. Mainly, an increase in fuel aromatic content was found to increase non-volatile particle numbers (Brem et al., 2015; Corporan et al., 2011, 2007; DeWitt et al., 2008; Lobo et al., 2011; Timko et al., 2010). A higher hydrogen content in fuel resulted in a reduction in non-volatile particles as well (Corporan et al., 2011, 2007). Additionally, an increase in fuel sulfur content was found to increase volatile particle numbers while non-volatile particle numbers were relatively unaffected (Brock et al., 2000; Petzold et al., 1999; Schröder et al., 2000, 1998; Schumann et al., 2002, 1996). Contrails were also found to have an effect on particle numbers as a lower number of particles were measured in the presence of contrails (Brock et al., 2000).

1.6 Objective

The objective of this thesis is to showcase a new aircraft emissions measurement system to measure both total and non-volatile particle number concentrations and using NO_x to calculate emission indices. Additionally, since there is little data on aircraft particle number emission

indices from in-flight experiments, particle number emission indices for conventional jet fuel and alternative biofuels are presented.

1.7 Overview

Chapter 2 outlines the general experimental set-up and details the methodology for the calculation of the particle number emission index including the Boeing Fuel Flow method (DuBois and C. Paynter, 2006). Detailed line losses considered and the uncertainty analysis are also presented. The results from the Civil Aviation Alternate Fuels Contrail and Emissions Research project (CAAFCER) are also reported. The flight campaigns were conducted in 2017 and jet engine exhausts from regular Air Canada commercial passenger flights were sampled at cruise under contrail conditions. Both conventional Jet A1 fuel and a 43% HEFA blend were used.

Chapter 3 describes the results from the Civil Aviation Alternate Fuels Contrails and Emissions with high Blend Biojet (CAAFCEB) campaign. The flights were conducted in 2018 sampling contrails from a source aircraft burning the three different fuels: conventional Jet-A1, conventional JP-5 and an alcohol-to-jet (ATJ) fuel blend. The ratio of the particle number emission indices of the ATJ and JP-5 relative to the Jet-A1 were determined and presented.

Chapter 4 presents a summary of the results and conclusions and any recommendations for future work that can be done to build upon and further improve the understanding of the relationship between aircraft particle emissions and alternative fuels.

Chapter 2 Civil Aviation Alternate Fuels Contrail and Emissions Research project (CAAFCER)

Although many ground-based studies have been completed to measure particle emissions from aircraft engines and a limited amount of studies done with aircraft in-flight, most were in either controlled test environments or using research specific aircrafts. The Civil Aviation Alternate Fuels Contrail and Emissions Research project (CAAFCER) was created to gather in-flight data from commercial aircraft operating during regular scheduled service using both conventional Jet A1 fuel and a 43% HEFA/Jet A1 blend.

2.1 Materials and methods

2.1.1 Experimental setup

The CAAFCER flight campaign was conducted in April/May 2017 and jet engine exhausts from Airbus A320 passenger jet airliners were sampled at cruise under contrail conditions. The sampled flights were part of regular Air Canada commercial passenger flights travelling between Toronto and Montreal, Canada. Table 2 shows the summary of the tests and the corresponding engine and fuel type. The Montreal-Toronto flights used the biofuel blend while the Toronto-Montreal flights used Jet A1 fuel. Flights were scheduled on days when contrail conditions were forecasted, and all measurements were made under contrail conditions. The National Research Council (NRC) Canada CT-133 jet aircraft flew in and out of the contrails in order to capture contrail and background data. The average age of contrails sampled was around 180 seconds.

The HEFA biofuel was produced by Alt-Air Fuels using used cooking oil as the feedstock and was blended with Jet A1 to create a mixture of 43% HEFA by volume. As

mentioned in Chapter 1.4, the ASTM D7566-19 standard allows for Jet A1 fuel to be blended with up to 50% HEFA biofuel for use in aviation turbines. The standard also requires the HEFA biofuel and biofuel blend to meet certain requirements with regards to properties such as aromatic content and fuel freezing point. Every biofuel flight used the same HEFA blend whereas each Jet A1 flight was fueled from a different source, thus the fuel samples from each flight were analyzed to determine the fuel properties such as hydrogen, aromatics, and sulfur content. The fuel properties are summarized in Table 2.sulfur

Table 2. Summary of tests and aircraft, engine, and fuel type used in each flight.

Date	Aircraft	Engine	Fuel Type	Hydrogen Content (% mass)	Aromatic Content (% volume)	Sulfur Content ppmm)
04-May-17 AM	A320	CFM56-5B4/P	Jet A1	13.7	18.6	700
04-May-17 PM	A320	CFM56-5A1	Jet A1	13.8	18.1	300
04-May-17 PM	A320	CFM56-5A1	43% HEFA	14.6	10.1	520

The instruments were housed in pods mounted under both wings of the CT-133. The instruments of interest were located in the starboard pod which is shown schematically in Figure 4. The sample entered through an isokinetic probe that was positioned in the direction of travel and led to a manifold. Two condensation particle counters (CPC) which measured particle concentrations drew samples from the manifold. The first CPC (TSI Inc., Model 7610) had a nominal cut-off diameter, d_{50}, of 15 nm while the second CPC (TSI Inc., Model 3776) had a d_{50} of 2.5 nm. Additionally, a catalytic denuder (Catalytic Instruments, Model CS015) that was in-line with the Model 3776 CPC, allowed for the measurement of non-volatile particles along with a bypass for the measurement of total particle number. Pinch valves were used to switch between

the catalytic denuder and bypass line for particles entering the 3776 CPC. A NO_x analyzer (Thermo Fisher Scientific, Model 42i) had a separate inlet that was located on the other side of the pod with the inlet facing the opposite direction of the travel. The exhausts from all three instruments were sent to the exhaust line where the sample flows were expelled.

The catalytic denuder removed volatile particles from the sample flow by evaporating the volatile particulate matter and oxidizing the resulting gas phase components. In this study, the temperature set-point of the catalytic denuder was set such that the temperature remained above 300 °C at all times during the flight (the temperature ranged between 300 and 380 °C for all flights).

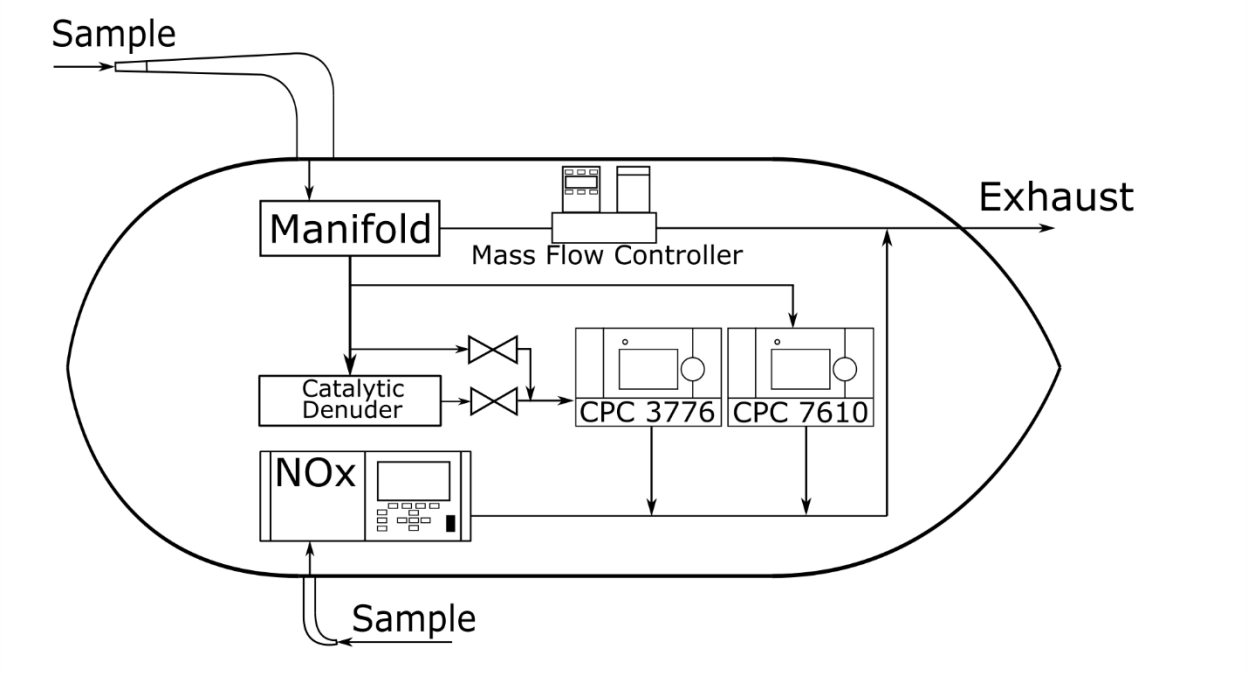

Figure 4. Layout of main instrumentation and plumbing in starboard pod.

2.1.2 Particle transport and counting efficiency in the isokinetic sampling system and Particle Counters

Particle losses through the sampling lines are important because it will affect the particle concentrations measured by the CPCs resulting in fewer particles detected by the CPCs than actual particles in the sample flow. The counting efficiencies of the CPCs can also be affected as particles below a certain size may not be able to fully penetrate the sampling lines which increases the 'effective' cut-off diameters of the CPCs.

2.1.2.1 Particle transport efficiency through the sampling system

A schematic of the isokinetic sampling system of the National Research Council Canada (NRC) CT-133 jet aircraft is shown in Figure 5. The sample flow enters the system through an isokinetic probe which consists of a conical tip and a bent tube (Section 1). The conical tip is attached to a stainless-steel tube comprised of a straight length and a 90° bend. The sample flow subsequently enters a coupler after the first section, which has a 90° elbow. The flow is then directed through Section 2 of the sampling system consisting of a conductive flexible tube that is bent at two points with bending angles of 20° and −20°. The sample is drawn through a manifold, where a small fraction of the sample is directed towards the lines leading to both particle counters and the rest of the sample flows to the mass flow controller and bulkhead exhaust. After the manifold, the sample enters Section 3 which consists of an elbow and a straight stainless-steel tubing connected to an additional length of flexible conductive tubing leading to a Y fitting that splits the sample flow to both condensation particle counters. Section 4 leads the sample to the TSI Model 7610 CPC. Section 5 leads to a second Y fitting which splits the flow between the catalytic denuder and the bypass line to the TSI Model 3776 CPC. Both Sections 6 and 7 contain pinch valves that are used to control whether the sample goes through

the catalytic denuder (Section 6) to measure non-volatile particles or the bypass line (Section 7) to measure total particles. Section 8 is the last section of the particle sampling system which leads the sample to the TSI Model 3776 CPC. Table 3 shows a summary of the total lengths and inner diameters for each section.

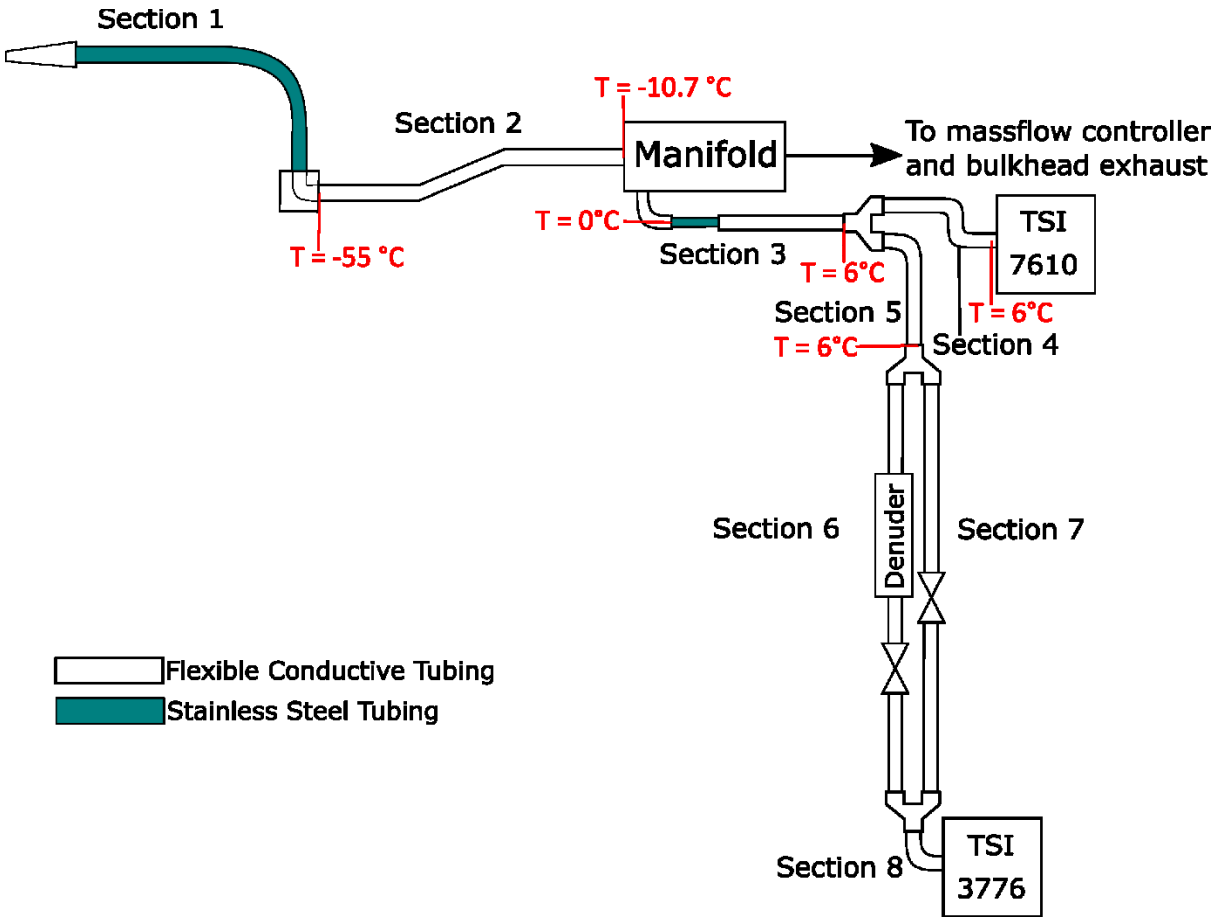

Figure 5. Schematic of the particle sampling system.

Particle losses in the system will be a function of the particle size. We assume contrail particles that will be measured by the system will consist of a small soot particle core (with diameters less than 100 nm) and a shell of frozen water at very low temperatures at high altitudes. Therefore, it is important to consider the effect of pod temperature on the sampled

particles and their estimated size as they enter the particle counter. It is known from previous experimental conditions that at top-of-climb, the pod temperature is ~20 °C and at top-of-descent, the pod temperature is ~6 °C. A pod temperature of 6 °C is considered in this study as the worst-case scenario for the effect of temperature on sampled particles. A heat transfer analysis was conducted on flow temperature as it traveled through the sampling system. Figure 5 shows the estimated flow temperature for various sections of the sampling system which are also summarized in Table 3. The flow temperature also affects air properties, such as density, viscosity, and volumetric flow rate, in different sections of the sampling system which, in turn, affect particle loss. Figure 5 shows that up to the manifold, the flow temperature is below zero and the water in the contrail particles will not evaporate; however, at the beginning of Section 3, the flow temperature reaches zero and increases up to 6 °C (*i.e.* pod temperature) at the end of that tube. Calculations show that the residence time of particles in Section 3 is much larger than their evaporation time. Therefore, particles reach the particle counter as soot with no condensed water vapour on them.

Three mechanisms for particle loss in the sampling system are considered: Diffusion loss in the tubes, inertial deposition loss in the bends and losses through the catalytic denuder. The extent of particle loss in each mechanism depends on the flow regime in the probe. Therefore, Reynolds number is an important parameter to consider when calculating particle loss in the probe. Because eddies do not form in expansions with a half angle less than 4°, inertial deposition particle loss is negligible in the conical tip (Kulkarni et al., 2011). However, diffusion loss must be still considered for the conical tip.

Figure 5 also shows a simplified model of the actual sampling system for the estimation of particle losses. As it will be shown later, diffusion losses depend on tube length; therefore, the

overall length of conical tip and the bent tube was considered as 610 mm for diffusion loss calculations. The overall straight section of the stainless-steel tube was 330 mm long, which was used to estimate inertial deposition losses in straight tubes.

Based on flight data, it was assumed that the isokinetic probe was at ambient conditions of −55 °C and 23 kPa. The rest of the sampling system was in a heated pod at 6 °C; however, it took some time for the sampled flow to heat up to the pod temperature. In the particle loss analysis, the flow temperature was assumed to be −55 °C in Section 1, an average of −33 °C in Section 2, and average of 3 °C in Section 3, and 6 °C in Sections 4 to 8. The density and viscosity of the air was calculated based on the temperature in each section. Assuming that the mass flow controller regulated the volumetric flow rate at 25 litres per minute at ambient pressure and temperature, Reynolds number was calculated to be 1,274 and 1,326 in Section 1 and Section 2, respectively. Therefore, the flow was laminar in both Sections 1 and 2. The particle counters both draw in a volumetric flow rate of 1.5 L/min (at 23 kPa and 6 °C) via their own pump. Thus, the Reynolds number in the stainless-steel tube and the conductive tubing of Section 3 was 166 and 110, respectively. The Reynold's number in Sections 4 to 8 was 55 and, therefore, the flow regime in all the remaining sections was laminar as well.

Table 3. Summary of each section of the sampling system.

Section	Total length (mm)	ID (mm)	Flowrate (L/min)	Temperature (°C)	Reynolds number
1	610	10.7	25	-55	1274
2	483	9.5	25	-33	1326
3 (Steel)	190.5	4.3	3	3	166
3 (Conductive tubing)	165	9.5	3	6	110
4	76	9.5	1.5	6	55
5	210	9.5	1.5	6	55
6	585	9.5	1.5	6	55
7	832	9.5	1.5	6	55
8	127	9.5	1.5	6	55

2.1.2.2 Diffusion Loss

Kulkarni et al. (2011) suggests the following set of equations to calculate transport efficiency (*i.e.* penetration) due to diffusional loss:

$$P_{\text{diff}} = \exp(-\xi \cdot \text{Sh}) \tag{2}$$

$$\xi = \frac{\pi D L}{Q} \tag{3}$$

where L is the tube length, Q is the volumetric flow rate, and D is the particle diffusion coefficient. Sherwood number, Sh, for laminar flow is calculated by the following empirical equation

$$\text{Sh}_{\text{laminar}} = 3.66 + \frac{0.0668\frac{d}{L}\text{Re}\cdot\text{Sc}}{1 + 0.04\left(\frac{d}{L}\text{Re}\cdot\text{Sc}\right)^{2/3}} \tag{4}$$

Reynolds number, Re, and Schmidt number, Sc, in Eq. 4 is defined as

$$\mathrm{Re} = \frac{\rho U d}{\mu} \tag{5}$$

$$\mathrm{Sc} = \frac{\mu}{\rho D} \tag{6}$$

where d is the inner tube diameter. Particle diffusion coefficient, D, is defined by

$$D = \frac{kTC_\mathrm{c}}{3\pi\mu d_\mathrm{p}} \tag{7}$$

where, C_c is the Cunningham slip correction factor (significant for particles in the range of or smaller than the mean free path of the air molecules) and d_p is the particle diameter. The mean free path of air molecules, λ, was calculated using (Willeke, 1976)

$$\lambda = \lambda_0 \left(\frac{T}{T_0}\right)\left(\frac{P_0}{P}\right)\left(\frac{1+\frac{S}{T_0}}{1+\frac{S}{T}}\right) \tag{8}$$

where P is the pressure, T is the temperature, S is the Sutherland constant (S = 110 K for air) (Willeke, 1976) and λ_0, P_0 and T_0 are the reference mean free path, pressure and temperature respectively. At a reference temperature and pressure of T_0 = 293.15 K and P_0 = 101.3 kPa, the mean free path is λ_0 = 0.0665 μm (Kulkarni et al., 2011). At a pressure of 23 kPa and temperatures of -55 °C and 6 °C, the mean free path of air molecules was estimated to be ~199 nm and ~275 nm, respectively. The Cunningham slip correction factor was calculated using (Kulkarni et al., 2011):

$$C_c = 1 + \frac{\lambda}{d_p}\left(2.33 + 0.966\exp\left(-0.499\frac{d_p}{\lambda}\right)\right) \quad (9)$$

2.1.2.3 Inertial Deposition in the Bend

Pui et al. (1987) gives the following empirical relation for inertial deposition in a laminar flow through a bend:

$$P_{\text{depos, laminar, bend}} = \left(1 + \left(\frac{Stk}{0.171}\right)^{0.452\left(\frac{Stk}{0.171}\right)+2.242}\right)^{-\frac{2}{\pi}\theta} \quad (10)$$

$$\text{Stk} = \frac{\tau U}{d} \quad (11)$$

where Stk is the Stokes number and θ is the angle of the bend in radians. In Eq. 11, τ is the relaxation time, U is the flow velocity and d is the tube diameter.

2.1.2.4 Losses in the Catalytic Denuder

The losses in the Catalytic Instruments, Model CS015 denuder was modeled by using the provided equation in the instrument manual ("Catalytic Stripper Manual," 2016)

$$P = \left(x_1 e^{-\frac{x_2}{{d_p}^2}} + x_3 e^{-\frac{x_4}{{d_p}^2}}\right)x_5 \quad (12)$$

where d_p is the particle diameter (in nm) and $x_1 - x_5$ are fitting parameters with the values shown in Table 4.

Table 4. Fit parameters for Eq. 12.

Parameter	Value
x_1	0.190
x_2	499
x_3	0.925
x_4	36.0
x_5	0.670

The resulting penetration efficiency curve is shown in Figure 6. As can be seen in Figure 6, the catalytic denuder has a maximum penetration efficiency of 75% once particles reach 100 nm or larger. Therefore, the measurement of non-volatile particles will experience a large amount of losses due to the denuder.

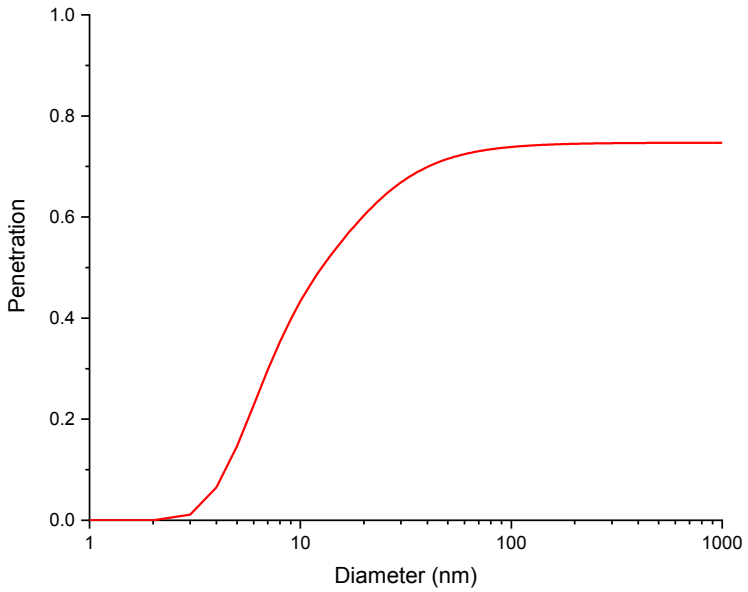

Figure 6. Penetration efficiency of particles in the catalytic denuder.

2.1.2.5 Counting Efficiency of the Particle Counters

The cut-off diameters of the counting efficiency of the TSI 3776 CPC and TSI 7610 CPC were found by fitting data provided in the TSI Model 3776 manual (TSI, 2011) and data estimated from Zhang and Liu (1991) for standard condition operation; respectively. A sigmoidal logistic fit was applied with the form shown in Eq. 13 and the parameters for both CPCs are shown in Table 5.

$$y = \frac{1}{1 + e^{-k(x-x_c)}} \tag{13}$$

Table 5. Parameters for logistic fit for both CPCs.

Parameters	TSI 3776	TSI 7610
k	7.11741	0.38999
x_c	2.27708	14.82943

The resulting counting efficiencies of the TSI 3776 CPC and the TSI 7610 CPC are shown in Figure 7. The 3776 CPC also has a much smaller cut-off diameter, d_{50}, of 2.5 nm compared to the 7610 CPC d_{50} of approximately 15 nm.

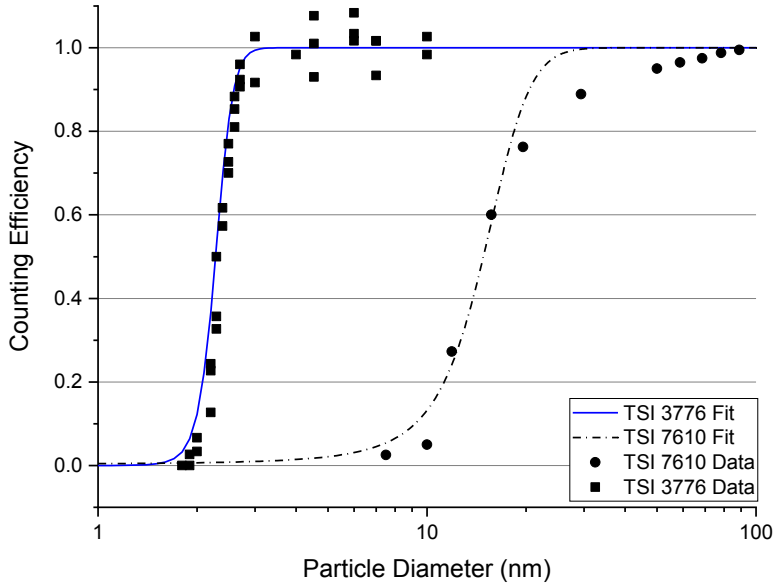

Figure 7. Counting efficiency of TSI 3776 and 7610 CPCs.

2.1.2.6 Overall Counting Efficiency of the Sampling System and Particle Counters

The overall penetration of particles through the sampling system takes into account the three different particle loss mechanisms in each tube section and bends, the catalytic denuder as well as the counting efficiency of the CPCs and was calculated using

$$P_{\text{overall}} = \frac{n_{\text{out}}}{n_{\text{in}}} = P_{\text{diff}} \times P_{\text{depos, bend}} \times P_{\text{denuder}} \times P_{\text{CPC}} \quad (14)$$

This assumes that the particle concentration is uniformly distributed across the tube at the entrance to each section.

2.1.2.7 Sampling System Particle Loss Results

Figure 8 shows the overall penetration of particles through the system before reaching the CPCs. It can be seen that with the current geometry, particle losses in the lines leading to the TSI 7610 CPC are the lowest with a d_{50}, the cut-off diameter (where the penetration efficiency is 50%), of 3.5 nm. For the bypass line leading to the TSI 3776 CPC, the d_{50} is slightly larger at

7.7 nm. Finally, the catalytic denuder has the largest impact on the penetration efficiency by reducing the maximum penetration efficiency to 75%, which leads to the largest d_{50} of 13.3 nm.

It should be noted that particle loss is negligible for the straight sections because the flow regime is laminar. Nevertheless, particle loss due to deposition in bends is still important mainly for particles larger than 10 μm. We expect particles in Sections 1 and 2 of the sampling system to contain contrail particles larger than 1 μm because these sections are not sufficiently warm to evaporate the condensed water; however, deposition loss in the bends is negligible for particle sizes up to 3 μm. Therefore, diffusional losses are the most significant contributor to the penetration efficiency of most particles through the sampling system. Due to the higher temperature of the flow in Sections 3–8, all water will evaporate and only soot particles survive, which generally have a median size less than 100 nm (Moore et al., 2017; Zhang et al., 2019). As seen in Figure 8, the sections leading to the TSI 7610 CPC and the bypass line leading to the TSI 3776 CPC have negligible particle losses for particles larger than 100 nm but the penetration efficiency begins to drop as the particle diameter decreases. As mentioned, the line including the catalytic denuder and leading to the TSI 3776 CPC has a penetration efficiency of 75% and has greater particle losses compared to the other two lines.

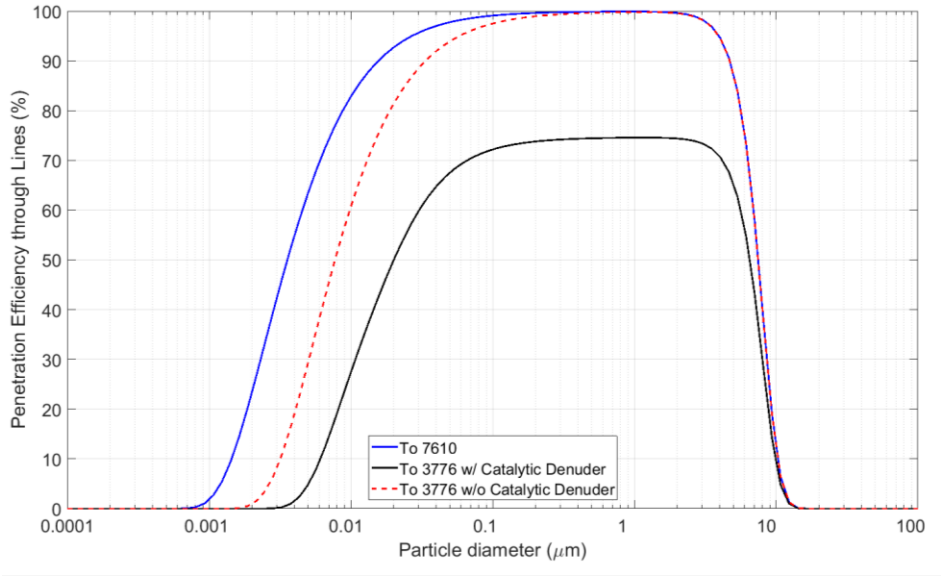

Figure 8. Overall particle penetration efficiency in the sampling system before the CPCs

Figure 9 shows the total counting efficiency of the sampling system including the counting efficiency of the CPCs. The resulting effective d_{50} of the TSI 3776 CPC and sampling system became 7.7 nm and 13.3 nm for the bypass line and catalytic denuder line, respectively. On the other hand, the effective d_{50} of the TSI 7610 CPC and sampling system remained relatively unchanged at 15.4 nm.

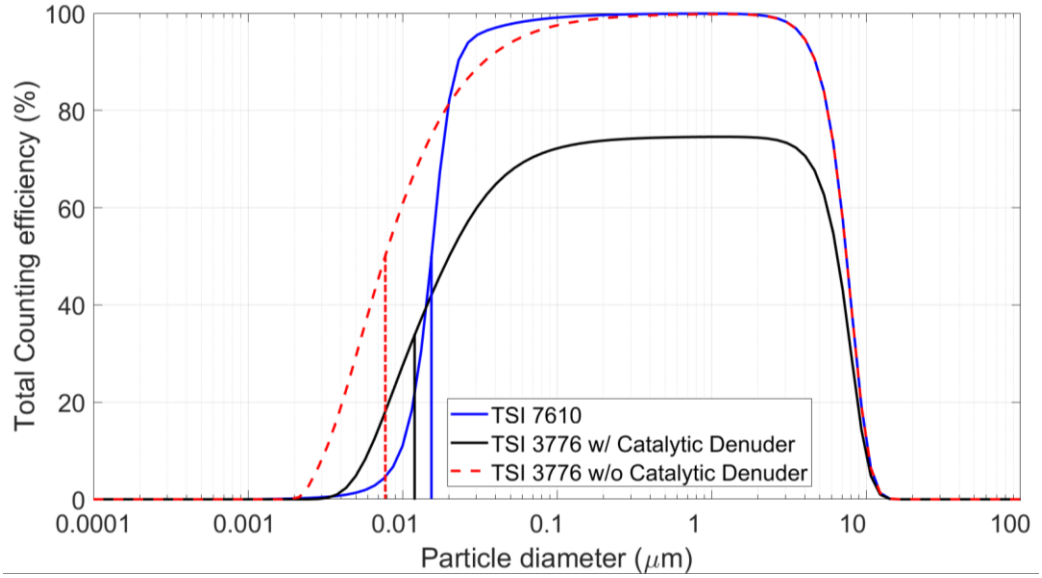

Figure 9. Total overall counting efficiency as measured by the CPCs.

It is important to note that the particle concentration measurements were not corrected for the losses in the lines because the size distribution of particles was not known, but the non-volatile particles were corrected for the 25% loss of particles through the catalytic denuder.

2.1.3 Methodology to determine particle number emission index

The CT-133 aircraft flew through aged contrails which meant the measurements were made in highly diluted plumes. To determine the particle number emission index (EI_N, the number of particles generated per mass of fuel burned), NO_x was used as a tracer similar to Anderson B. E. et al. (1999) and Febvre et al. (2009). CO_2 is often used as a tracer (Anderson B. E. et al., 1998; Brock et al., 2000; Moore et al., 2017; Schröder et al., 2000, 1998), but NO_x was preferred in this study because the NO_x analyzer and both CPCs were co-located in the same wing-mounted pod. The other benefit is that because the plume was relatively dilute, the NO_x measurements had a better signal-to-noise ratio compared to CO_2. The particle number emission index was determined by (Anderson B. E. et al., 1999):

$$EI_N = \frac{\Delta N\, C(N)}{\Delta y_{\mathrm{NO_x}}} EI_{\mathrm{NO_x}} \tag{15}$$

where EI_{NOx} is the NO_x emission index, and ΔN and Δy_{NOx} are the background-subtracted concentration measurements of particles and NO_x, respectively. $C(N)$ is a unit-conversion factor defined as follows:

$$C(N) = \left(\frac{1}{M_{\mathrm{NOx}}}\right)\left(\frac{RT_{\mathrm{CPC}}}{P_{\mathrm{CPC}}}\right) \tag{16}$$

where R is the ideal gas constant, T_{CPC} and P_{CPC} are the operating temperature and pressure of the CPC, and M_{NOx} is the molar mass of NO_x (which was taken as equivalent to the molar mass of NO_2 (Schulte P. et al., 1997)). The temperature within the CPC was taken to be constant at T_{CPC} = 21 °C as this is the standard condition used by the instrument manufacturer for flow measurement (Wang and Horn, 2008) and the pressure, P_{CPC}, was the value measured by the CPC at the CPC inlet.

The emission index of NO_x at altitude, EI_{NOx}, was calculated using Boeing's Fuel Flow Method 2 (DuBois and C. Paynter, 2006). This method provided an estimate for the NO_x emission index at the outlet of the jet turbine engine exhaust at cruise conditions as a function of fuel flow rate. Boeing's Fuel Flow Method 2 was used since only emission data at sea level is publicly available but emissions at altitude are needed. In brief, the fuel flow method determines the NOx emission index at altitude, $EI_{\mathrm{NOx,ALT}}$, by

$$EI_{\mathrm{NO_x,ALT}} = EI_{\mathrm{NO_x,SL}} \left(\frac{\delta_{\mathrm{amb}}^{1.02}}{\theta_{\mathrm{amb}}^{3.3}}\right)^{0.5} e^{H} \tag{17}$$

where $EI_{\mathrm{NOx,SL}}$ is the NO_x emission index at sea level, H is the humidity correction factor, and θ_{amb} and δ_{amb} are the dimensionless temperature and pressure defined as

$$\theta_{\text{amb}} = \frac{T_{\text{amb}}}{518.67\ °\text{R}} \tag{18}$$

$$\delta_{\text{amb}} = \frac{P_{\text{amb}}}{14.696\ \text{psia}} \tag{19}$$

where T_{amb} and P_{amb} are the ambient temperature (in °R) and pressure (in psia) at altitude, respectively. The humidity correction factor, H, is represented by

$$H = -19(\omega - \omega_o) \tag{20}$$

where ω is the humidity ratio and ω_o is the humidity ratio of dry air at sea level standard day conditions (ω_o = 0.00634 kg H_2O/kg dry air). The value of ω_o corresponds to a relative humidity of 60% which the fuel flow method assumed for the ICAO Emissions Databank data. The humidity ratio, ω, is calculated by Eqs. 7 and 8 from ISO 5878 Addendum 2,

$$\omega = \frac{0.62197058\ RH\ P_{\text{sat}}}{\left(\left(P_{\text{amb}}\ 68.9473\,\frac{\text{mbar}}{\text{psia}}\right) - (RH\ P_{\text{sat}})\right)} \tag{21}$$

$$P_{\text{sat}} = (6.107\ \text{mbar})\ 10^{\left(\frac{7.5\times T_{\text{amb}}}{237.3+T_{\text{amb}}}\right)} \tag{22}$$

where RH is the relative humidity, P_{sat} is the saturation vapour pressure, and T_{amb} is the ambient temperature (in °C) (ISO 5878, 1990).

To determine the NO_x emissions index at sea level, $EI_{\text{NOx,SL}}$, the equivalent fuel flow rate at sea level, $W_{\text{f,SL}}$, was needed which is given by

$$W_{\text{f,SL}} = W_{\text{f,ALT}} \frac{\theta_{\text{amb}}^{3.8}}{\delta_{\text{amb}}} e^{0.2\,M^2} \tag{23}$$

where $W_{\text{f,ALT}}$ is the fuel flow rate at altitude and M is the Mach number of the source aircraft.

The ICAO Aircraft Engine Emissions Databank (2019) provides four points of data for the fuel flow rates and emissions indexes, corresponding to the landing and takeoff (LTO) cycle:

takeoff, climb-out, approach, and idle/taxi. Thus, determination of the NO_x emissions index required interpolation. As per Boeing's Fuel Flow Method 2, a linear log-log fit between each pair of points was used. The calculated fuel flow at altitude and the data points for fuel flow and emission indices were converted into logarithmic base 10 form. Then a linear interpolation was performed using the calculated fuel flow at sea level to determine the corresponding emission index of NO_x at sea level.

To account for the environmental control system (ECS) bleed effect on the fuel flow, an installation correction factor was developed by Boeing and the values are shown in Table 6. These correction factors were applied first to the fuel flow rate values taken from the ICAO Emissions Databank before being converted to log base 10.

Table 6. Fuel flow installation correction factors for each landing and take-off (LTO) operational mode.

LTO Mode	Installation Correction Factor
Takeoff	1.010
Climb-out	1.013
Approach	1.020
Idle/Taxi	1.100

Flight conditions such as altitude, Mach number, fuel flow rate (at altitude), and ambient temperature data were recorded by the source aircraft. The ambient pressure was not measured but was estimated using the ICAO Standard Atmosphere model (ICAO, 1993) which provided ambient pressure as a function of altitude.

2.1.4 Flight segment selection

The data from the instrumentation aboard the CT-133 aircraft was collected throughout the entirety of the flight on each day. Due to various instrument malfunctions and data losses during the campaign, only a fraction of the flights completed were analyzed. Most flights had approximately seven individual segments with a few flights only containing one or two segments which were analyzed. For the case of the 3776 CPC, these segments would be split between total and non-volatile particles. Since the instruments had different sample transit times, the data from the instruments were time-aligned to match the peaks in concentrations of particles and NO_x. Only the exhaust measurements sampled when the source aircraft was at cruise were considered and this was determined by observing the fuel flowrate recorded by the source aircraft. Next, within each denuded and non-denuded section, the background concentrations for each section were determined by removing all obvious concentration peaks and fitting a line of best fit over the remaining data points and taking the value at the mid-point of the data section. The background values were then subtracted from their respective sections and periods with concentrations above the background were chosen for the analysis (segments ranged from 5 s to 30 s long). The uncertainty in determining the background concentration was included in the uncertainty analysis.

Since each instrument had different response times, the ΔN, Δy_{NOx}, P_{CPC}, and EI_{NOx} terms in Eqs. 15 and 16 were replaced with their respective integrals over the time of the measurement segment for the calculation of the particle number emission index, EI_N, following the method of Schulte P. et al. (1997).

2.1.5 Uncertainty analysis

From Eq. 15, the ΔN and Δy_{NOx} terms can be expanded to become:

$$EI_{\mathrm{N}} = \frac{\left(N - N_{\mathrm{bg}}\right)C(N)}{y_{\mathrm{NO_x}} - y_{\mathrm{NO_x bg}}} EI_{\mathrm{NO_x}} \tag{24}$$

A Monte Carlo simulation was performed using the bias uncertainties for the particle number, N, background particle number, N_{bg}, NO_x concentration, y_{NOx}, NO_x background concentration, y_{NOxbg}, and the NO_x emission index, EI_{NOx}. The uncertainties from the conversion factor shown in Eq. 24 were not included because the uncertainties in N, and EI_{NOx}, were expected to be much larger than the uncertainty in the conversion factor. The simulations also accounted for the precision uncertainty by combining multiple segments of the same case for each flight where possible. A cumulative distribution plot for the particle emission index was then created for each case to determine the 95% confidence intervals.

The manufacturer's accuracy specification for the TSI 7610 CPC is ±10 % of reading. Zhang and Liu (1991) performed tests on the 7610 CPC at reduced pressured and found that the counting efficiency only slightly decreases at 0.2-0.3 atm and only at pressures below 0.2 atm did the counting efficiency drop sharply. Thus, for the Monte Carlo simulation it was assumed that the uncertainty in the 7610 CPC was a Gaussian distribution with 2σ=±10 % of reading. The TSI 3776 CPC has the same uncertainty as the 7610 CPC as specified by the manufacturer, however a study by Takegawa et al. (2017) reported that the 3776 CPC overestimates particle concentrations by 20–40% for particles with mobility diameters of 11 and 48 nm at absolute inlet pressures of 102 and 60 kPa. Therefore, for the Monte Carlo simulation it was assumed that the uncertainty in the 3776 CPC was a Gaussian distribution with 2σ=±30 % of reading.

The uncertainty in the background values were calculated by taking half of the difference between the minimum and maximum background values of the line of best fit, represented as $\varepsilon_{N_{\mathrm{bg}}}$. The background particle concentration may be changing during the test as the background concentration is not expected to be constant throughout the atmosphere. It was assumed that there was an equal chance for the background value to fall anywhere between the upper and lower limits. Therefore, a square distribution was used for the background uncertainty.

The NO_x analyzer was calibrated over a range NOx concentrations and ambient pressures. Thus, the calibration curve of the NOx instrument is given as,

$$y_{\mathrm{NO_x}} = f_1(P)x + f_2(P) \tag{25}$$

$$f_1(P) = (-4.39 \times 10^{-7})P^3 + (3.35 \times 10^{-4})P^2 - (9.13 \times 10^{-2})P + 9.58 \tag{26}$$

$$f_2(P) = (7.87 \times 10^{-7})P^3 - (4.85 \times 10^{-4})P^2 + (9.3010^{-2})P - 4.98 \tag{27}$$

where x is the measured NO_x concentration and P is the ambient pressure in mmHg. Eq. 26 and 27 were trend lines fitted to data for the slopes (response factor) and intercepts (zero offset) of the instrument response at different pressures. These equations were applied to the measured NO_x concentrations before calculating the particle number emission index. In this case, the correlated source of error for y_{NOx} and $y_{\mathrm{NO_{x\,bg}}}$ come from the calibration equation in Eq. 25 and the uncertainty in the calibration becomes (ASME, 2013):

$$\varepsilon_{y_{\mathrm{NOx}}}^2 = \left(\frac{\partial y}{\partial f_1}\frac{\partial f_1}{\partial P}\right)^2 \varepsilon_{f_1}^2 + \left(\frac{\partial y}{\partial f_2}\frac{\partial f_2}{\partial P}\right)^2 \varepsilon_{f_2}^2 + \frac{\partial y}{\partial x}^2 \varepsilon_x^2 \tag{28}$$

where ε_{f_1} and ε_{f_2} are the uncertainties in Eq. 26 and 27, respectively, and were determined by finding the largest difference between the trend lines and actual data points. The calibration curves are shown in Figure 10 and Figure 11 and the values for ε_{f_1} and ε_{f_2} were 4.34×10^{-3} and 7.65×10^{-2}, respectively. The uncertainty in the measured NO_x concentration, ε_x was taken as the

uncertainty of the calibration gas used for the calibration of the NO_x analyzer (ε_x = 1%). Eq. 28 was then used to determine the uncertainty in the measured NO_x concentration, $\varepsilon_{y_{NO_x}}$. For the test conditions in this study $\varepsilon_{y_{NO_x}}$ ranged between 1.2% and 1.4%. In the Monte Carlo analysis, it was assumed that this uncertainty was Gaussian.

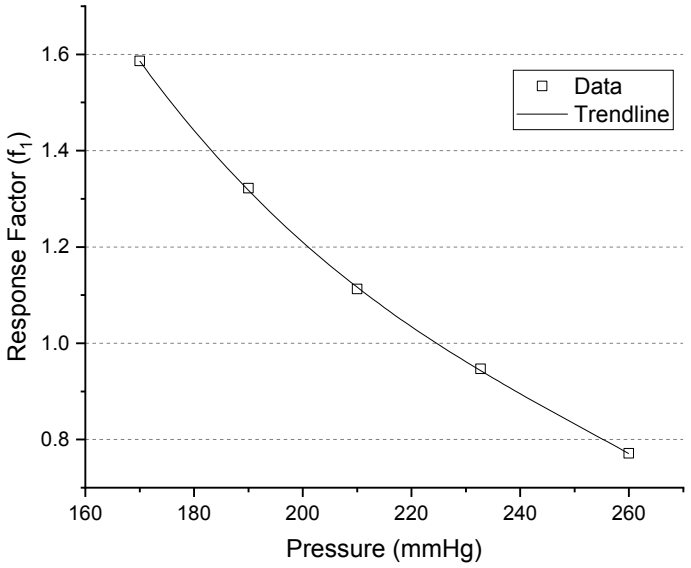

Figure 10. The NOx calibration response factor as a function of pressure.

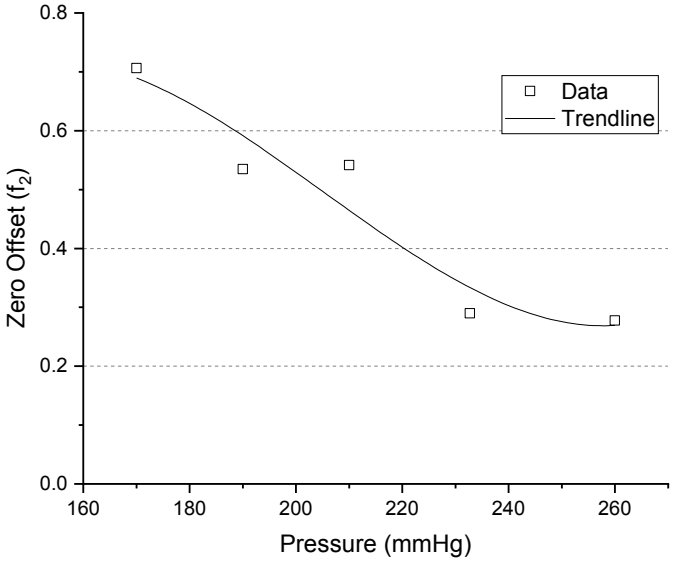

Figure 11. The NOx calibration zero offset as a function of pressure.

Similar to the particle concentration background uncertainty, the uncertainty in the NO_x background was determined by taking half of the difference between the minimum and maximum of the trend lines fitted to the approximated background data. Thus, a square distribution was used for the Monte Carlo simulation.

For the uncertainty in the NO_x emission index, the Fuel Flow Method 2 by DuBois and C. Paynter (2006) estimates the NO_x emissions within ±10% to ±15% from comparisons to inflight data. To be conservative, the uncertainty in EI_{NOx} was assumed to be Gaussian with 2σ=±15% of reading.

Sample histograms plots for the particle and NO_x concentration as well as background and EI_{NOx} results for one segment of the May 4 AM flight are shown in Figure 12.

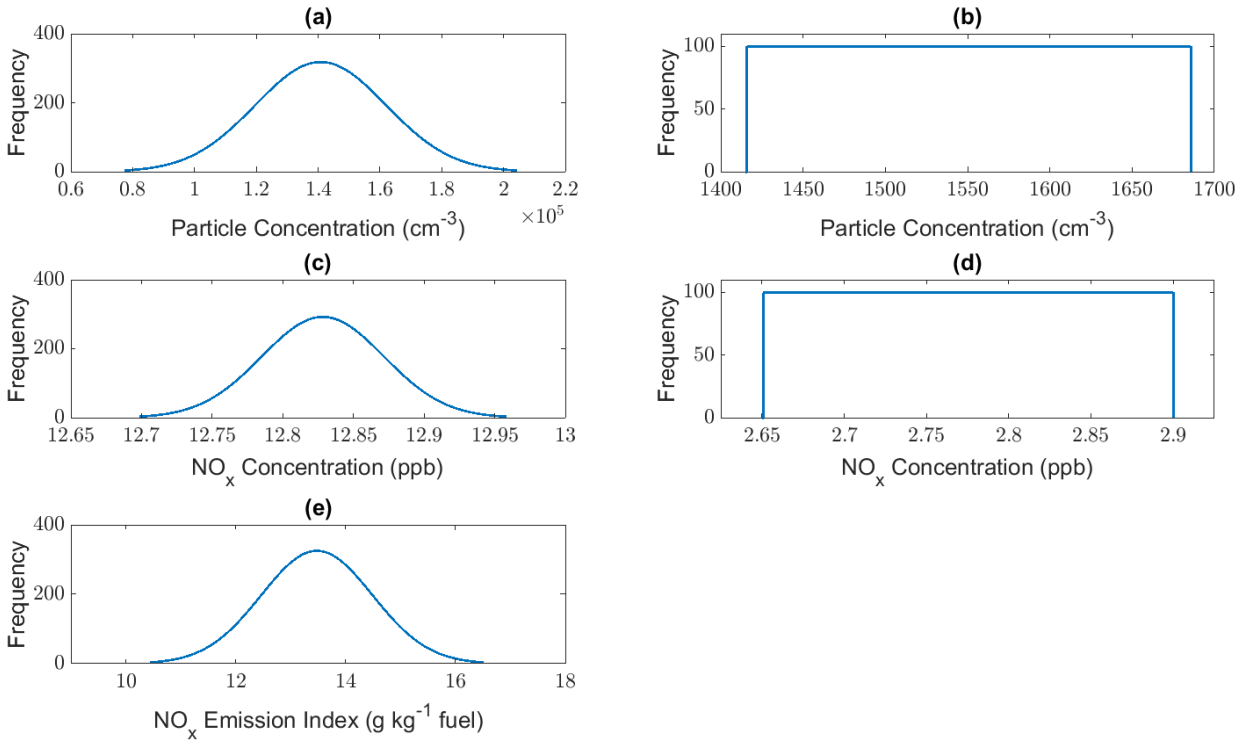

Figure 12. Sample inputs for the Monte Carlo Simulation for one segment of the May 4 AM flight: (a) particle number concentration (TSI 3776), (b) background particle concentration (TSI 3776), (c) NO_x concentration, (d) background NO_x concentration, and (e) NO_x emission index.

2.1.5.1 Monte Carlo Simulation

A Monte Carlo simulation was performed and implemented in Matlab. All the variables shown in Eq. 24, except for the conversion factor, were randomly selected from within their respective inputs as shown in Figure 12. These values were then used to calculate the particle number emission index. This calculation was repeated 10,000 times for each flight segment to create a frequency distribution of particle number emission indices. For the cases which included multiple segments, the distributions were combined to create an overall frequency distribution. From the frequency plots, a cumulative distribution was created from which the upper and lower limits were determined.

As an example, the May 4 morning flight included a total of six separate segments for both fuel cases. The resulting histogram plots for the particle emission index values from the Monte Carlo simulation are shown in Figure 13. Figure 13 also shows the corresponding cumulative distribution plots for both CPCs. By using the cumulative distribution plots, the upper and lower limits were taken at the 95% and 5% confidence interval levels, respectively. The multimodal distribution seen in Figure 13(c) is the result of aggregating the six segments to produce an overall distribution.

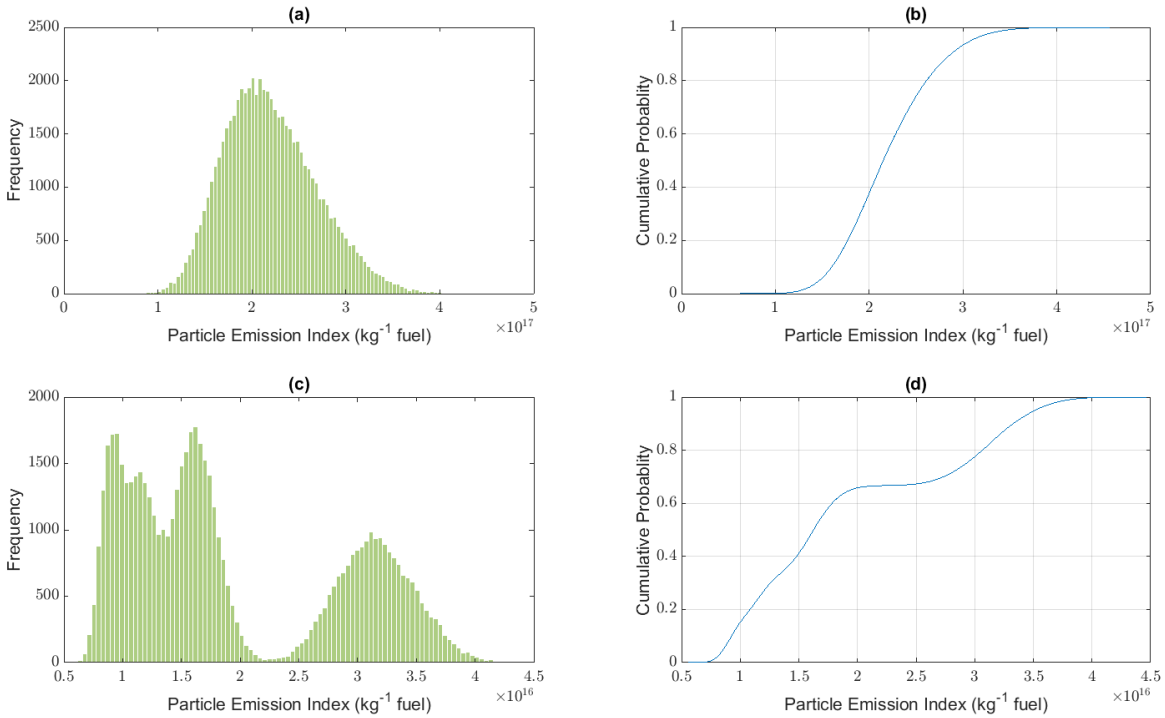

Figure 13. Monte Carlo results for the May 4 AM total particle emission index. (a) distribution for the TSI 3776 (b) cumulative distribution for the TSI 3776 (c) distribution for the TSI 7610 (d) cumulative distribution for the TSI 7610.

Since not all the cases had multiple segments, for the cases with only one segment, the relative confidence intervals from similar cases with more segments were applied. Figure 14 shows the results for all cases measured for the all the remaining flights. Table 7 summarizes the final results including the particle emission index and the corresponding confidence intervals for all flights.

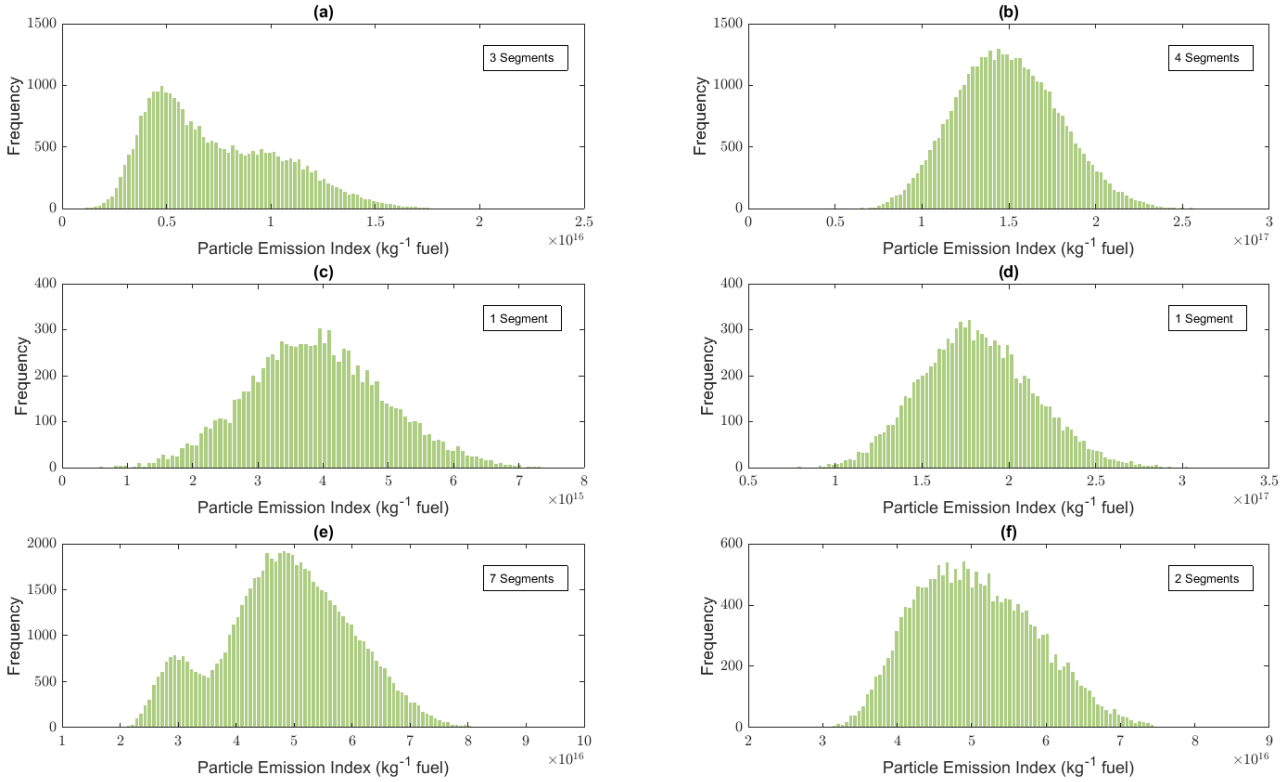

Figure 14. Distribution for all May 4 PM flights: (a) 3776 CPC HEFA blend non-volatile particles (b) 3776 CPC HEFA blend total particles (c) 3776 CPC Jet A1 non-volatile particles (d) 3776 CPC Jet A1 total particles (e) 7610 CPC HEFA blend total particles (f) 7610 CPC Jet A1 total particles.

Table 7. Summary of the final particle number emission index results for the CAAFCER campaign. The particle number emission index values were calculated using integrals and the confidence intervals were determined from the Monte Carlo simulation.

Flight	Fuel type	Particle type	Effective cut-off diameter (nm)	Particle number emission index (kg^{-1} fuel)	Uncertainty Upper limit (95%) (kg^{-1} fuel)	Uncertainty Lower limit (5%) (kg^{-1} fuel)
May 4 AM	Jet A1	Total	7.7	2.17×10^{17}	3.08×10^{17}	1.47×10^{17}
May 4 AM	Jet A1	Total	15.4	1.73×10^{16}	3.50×10^{16}	8.57×10^{15}
May 4 PM	43% HEFA	Non-Volatile	13.3	6.76×10^{15}	1.30×10^{16}	3.31×10^{15}
May 4 PM	Jet A1	Non-Volatile	13.3	3.55×10^{15}	5.69×10^{15}	2.22×10^{15}
May 4 PM	43% HEFA	Total	7.7	1.44×10^{17}	1.99×10^{17}	1.02×10^{17}
May 4 PM	Jet A1	Total	7.7	1.74×10^{17}	2.39×10^{17}	1.29×10^{16}
May 4 PM	43% HEFA	Total	15.4	4.62×10^{16}	6.67×10^{16}	2.86×10^{16}
May 4 PM	Jet A1	Total	15.4	4.73×10^{16}	6.48×10^{16}	3.84×10^{16}

2.2 Results and discussion

The particle number emission indices from the flights are summarized in Figure 15. The results include total particle number emission indices for particles with diameter $d_p > 7.7$ nm (for 3776 CPC) and $d_p > 15.4$ nm (for 7610 CPC) as well as the non-volatile particle number emission indices for particles with $d_p > 13.3$ nm (for 3776 CPC with catalytic denuder). It is important to note that conditions, such as fuel flow rate, ambient temperature and altitude for each of the tests shown in Figure 15 were slightly different but varied by less than 7%. These conditions are summarized in Table 8.

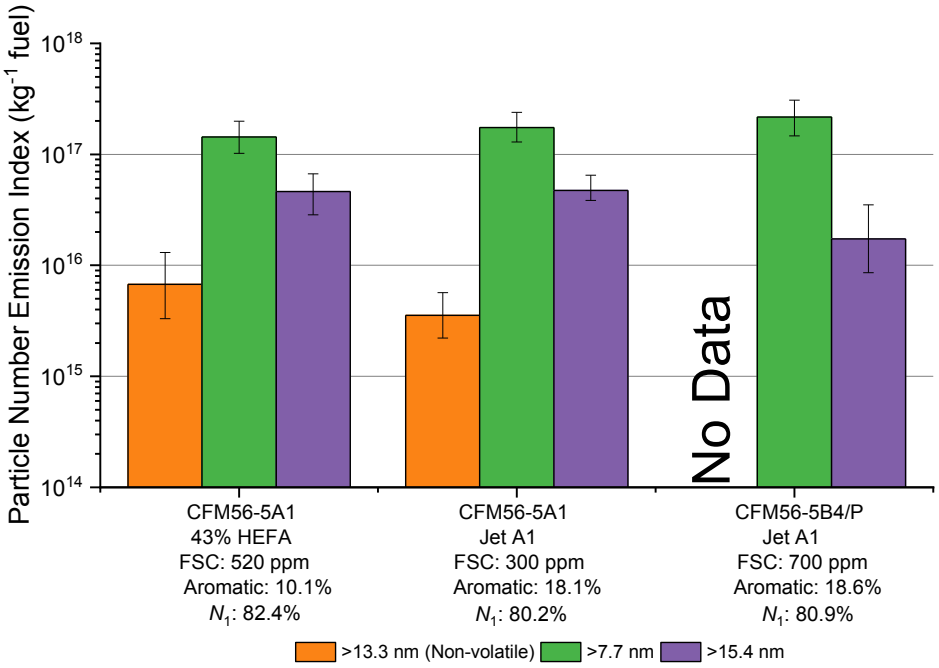

Figure 15. Calculated particle emission indices from CAAFCER. (FSC represents fuel sulfur content and N1 represents the engine gas generator rotational speed as a percentage of maximum). The error bars represent 95% confidence.

Table 8. Fuel and engine type and ambient flight conditions for each flight case.

Fuel and engine type	Measured particle size	Ambient Temperature (°C)	Altitude (m)	Fuel Flow (kg/hr)
43% HEFA CFM56-5A1	>15.4 nm	-50	9 820	1 270
	>7.7 nm	-50	9 820	1 280
	>13.3 nm (NV[a])	-50	9 830	1 250
Jet A1 CFM56-5A1	>15.4 nm	-48	9 500	1 220
	>7.7 nm	-48	9 500	1 200
	>13.3 nm (NV[a])	-47	9 500	1 230
Jet A1 CFM56-5B4/P	>15.4 nm	-48	9 540	1 250
	>7.7 nm	-48	9 540	1 250

[a] Non-volatile

Figure 3 shows a discernable difference between total and non-volatile particle numbers, which means that a very large fraction (~95-98% if neglecting the difference between the cut-off diameters between the two measurements) of the particle emissions are comprised of volatile particles. These results are in line with the findings from Anderson B. E. et al. (1998) who found that volatile particle concentrations were one to two orders of magnitude higher than non-volatile particle concentrations. Sources of volatile particles in aircraft emissions include nucleation aerosols formed from gas-phase components in the exhaust, most notably sulfur compounds which form sulfuric acid (Anderson B. E. et al., 1998; Schröder et al., 2000). Volatile particles are generally found in the sub-10 nm range (Schröder et al., 2000), which supports the increase in total particle numbers from $d_p > 15.4$ nm to $d_p > 7.7$ nm.

For the two Jet A1 cases, although they both used the same type of fuel, there is a difference in the fuel sulfur content and engine type. Fuel composition has been shown to have a significant influence on emissions. For example, it has been observed that reducing sulfur content from 1500 ppm to <100 ppm will yield substantial volatile particle number emissions reductions (Moore et al., 2015). Considering the overlap of the error bars between the two cases, the fuel sulfur content did not appear to have any discernable effect on the particle number emissions. Moore et al. (2017) reported similar findings that increasing the fuel sulfur content from 22 ppm to 416 ppm had no observable effect on the particle number. Similarly, Schröder et al. (2000) found that a large change in fuel sulfur content did not significantly affect particle numbers when the absolute fuel sulfur content value was small (results from fuels tested with fuel sulfur content between 2.6 and 118 ppm), although higher levels of fuel sulfur were used in these tests. Besides the fact that the two aircraft engines were different for each flight, there is

also the possibility that fuel sulfur content has a smaller effect on the evolution of emissions under contrail conditions compared to non-contrail conditions (Schumann et al., 2002).

Taking the uncertainties into consideration, the results do not show there is a discernable difference between the particle number emissions for the HEFA blend and Jet A1 of the CFM56-5A1 engines. With the difference in aromatic content between the two fuels as shown in Table 2, the HEFA blend would have been expected to provide a reduction in soot emissions as shown by previous studies (Brem et al., 2015; Corporan et al., 2011, 2007; DeWitt et al., 2008; Lobo et al., 2011; Timko et al., 2010). In this case, the biofuel alternative did not reduce the number of particles emitted per kilogram of fuel unlike the results from Moore et al. (2017) which showed the use of a 50:50 HEFA blend over Jet A1 fuel reduces the particle number emissions by 50%-70%. From Table 8, it can be seen that the ambient flight conditions for each of the cases were relatively similar with no significant difference in the ambient temperature, altitude, or fuel flow rate. Thus, the ambient conditions are not expected to contribute significantly to any differences observed between the emissions indices measured for each case. A likely factor for the absence of any trends observed with the change in fuel type could be due to the fact that the aircrafts were not identical for every case (although the aircrafts shared the same engine model). Different engine models may have different emissions indices and, moreover, it has been shown that the age of the engine can have an impact on the emissions as well (Lukachko and Waitz, 1997).

A number of different previously completed flight campaigns also reported particle number emission indices: ACCESS (Moore et al., 2017), SULFUR-2 (Schumann et al., 1996), SULFUR-5 (Schröder et al., 1998), SULFUR-6 (Schröder et al., 2000), SULFUR-7 (Schumann et al., 2002), SONEX (Anderson B. E. et al., 1999), PAZI-2 (Febvre et al., 2009), and SNIF-II and SUCCESS (Anderson B. E. et al., 1998). Using the reported particle number emission

indices from previous studies, the geometric means and geometric standard deviations (GSD) for total and non-volatile particle number emission indices were calculated. For total particles the geometric mean was found to be 7.93×10^{15} particles per kg of fuel, with a GSD of 6.8. For non-volatile particles the geometric mean was 9.27×10^{14} kg^{-1} with a GSD of 2.7. The large GSD in these measurements show that there is a great variability in in-flight emission indices, which may be caused by differences in engines, fuels, fuel sulfur content, operating conditions, the presence of contrails, CPC cut-off diameter, sampling system losses, and uncertainties in the measurements.

The non-volatile particle emission indices measured here have a geometric mean of 4.90×10^{15} kg^{-1} which is 5 times larger than the geometric mean of the other in-flight tests. In comparison, the geometric mean total particle number emission index from the results of this study is 7.68×10^{16} kg^{-1} (GSD = 2.5) which is about ~9 times larger than previous tests. As previously discussed, fuel sulfur content has been shown to increase volatile particle numbers (Anderson et al., 1998; Schumann et al., 2002). The geometric mean of the FSC for all the previous tests is approximately 50 ppm with a GSD of 7.2. However, in this study the FSC has a geometric mean of 478 ppm (GSD = 1.4). Thus, the total particle number emission index in this study is about an order of magnitude larger than the values from the literature but the corresponding FSC is also larger by an order of magnitude.

The cut-off diameter of a CPC will also affect particle number measurements because a smaller cut-off diameter allows for measurements of a larger range of particle sizes. As shown in this work, sampling line losses can be significant which effectively shift the cut-off diameter measured by the CPC to larger sizes. Previous studies often do not report the effective cut-off of their measurement systems which makes the comparison of data between sampling systems

difficult. As shown in Figure 3, a very large number of particles were between 7.7 nm and 15.4 nm in diameter. Thus, a small change in the effective cut-off of the sampling system can have a very large impact on the measured emission index. Thus, it is recommended that future studies of emission factors report the effective cut-off of their sampling system and CPC either through modeling the system as done here or by calibration as done by Cofer et al. (1998).

Particle numbers have also been shown to be affected by the formation of contrails. Greater coagulation is expected as small particles are scavenged by larger contrail ice crystals reducing the overall number of particles (Kärcher et al., 1998). The calculated geometric means for total and non-volatile particle number emission indices for previous studies include both measurements made in contrail and non-contrail conditions. Since the CAAFCER flights were sampled in contrail conditions, a decrease in particles would be expected compared to non-contrail conditions due to the implication that smaller particles would attach to the ice particles as they collide (Moore et al., 2017; Schröder et al., 1998; Schumann et al., 2002).

The age of the plume when sampled will also affect the particle numbers measured as total particle numbers may increase or decrease as plumes age depending on whether or not contrails form (Schröder et al., 1998). Anderson B. E. et al. (1999) found that the number of particles larger than 17 nm increase in time due to condensation of volatile material on small particles (larger than 8 nm). Schröder et al. (2000) found that in contrail-conditions, the number of particles larger than 3 nm slightly increased as plumes aged but the number of particles larger than 3 nm in dry (non-contrail) plumes were much greater (increased by factors of 5-10 in the first 2 seconds). This is likely due to coagulation of large ice contrail particles with smaller particles over time (Schumann et al., 2002). In high fuel sulfur cases, an increase in the number

of contrail particles may also be expected as water and sulfuric acid droplets are given more time to freeze (Petzold et al., 1997).

Zhang et al. (2019) developed a size-resolved BC particle number emission inventory by converting BC mass to number using fractal aggregate theory and particle mass parameters validated using data from previous in-flight experiments. From this inventory, Zhang et al. (2019) calculated an average non-volatile particle number emission index for cruise conditions of $(5.8\pm1.2) \times 10^{14}$ per kg of fuel burned for global civil aviation. The global average calculated by Zhang et al. (2019) is close to the geometric mean of previous in-flight studies of 9.27×10^{14} kg^{-1} with a of geometric standard deviation of 2.7. The large geometric standard deviation indicates that there is a large variability in in-flight emissions. This suggests emission inventories should be improved to account for differences in engines, fuels, fuel sulfur content, and operating conditions. This can be done by modelling, which must be validated with in-flight data. Thus, more in-flight data is needed spanning a range of engine, fuels, fuel sulfur content, and operating conditions.

Chapter 3 Civil Aviation Alternate Fuels Contrails and Emissions with high Blend Biojet (CAAFCEB)

As mentioned in Chapter 1.4, many ground- and flight-based studies have been previously completed to study the effects of fuel composition as well as alternative fuels on aircraft particle emissions. ASTM has approved a number of different synthetic biofuels that may be blended with up to 50% by volume with conventional Jet fuel (ASTM D7566-19, 2019). Alcohol-to-Jet (ATJ) is one of the certified alternative fuels which involve converting alcohol derived from organic feedstock into a jet fuel product that could replace conventional jet fuel. The technology is still in the early stages of development with only a few companies pursuing ATJ as an alternative source of fuel (Pechstein et al., 2018), and to our knowledge, only one lab-based study has been completed with a non-blended ATJ fuel which found a significant reduction in particle numbers compared to regular Jet A1 fuel (Schripp et al., 2019). The purpose of the Civil Aviation Alternate Fuels Contrails and Emissions with high Blend Biojet (CAAFCEB) project was to sample aircraft emissions in-flight to compare the effects of an ATJ blend and conventional JP-5 fuel to conventional Jet A1 fuel.

3.1 Materials and methods

3.1.1 Experimental set-up

Following the CAAFCER flight campaign, the CAAFCEB flights were completed by the National Research Council (NRC) Canada over the period of November 2017 to March 2018 using NRC's Falcon 20 (GE CF700-2D2 engines) as the source aircraft. NRC's CT-133 jet was used to capture contrail and emissions data under contrail conditions. The average age of contrails encountered was around 4 minutes (50 km in length).

The Falcon was fueled with two different fuels for each flight and a total of three different jet fuels were used: conventional Jet-A1, JP-5 and an alcohol-to-jet (ATJ) fuel blend. The wing tanks were filled with Jet-A1 fuel for all flights while the starboard engine fuel feeder tank was filled with either JP-5 or the ATJ blend. On each flight, the contrails from two different fuels were sampled by having the Falcon switch between the different fuel tanks to feed the engines. The ATJ fuel was blended with 8% of 150 Napthalene Depleted (ND) mono-aromatics by the NRC to condition the fuel for the Falcon fuel system. Aromatic content in the fuel is needed because it causes nitrile O-rings to swell preventing fuel leaks (Corporan et al., 2011; DeWitt et al., 2008). Samples were taken from each tank for each flight and analyzed. The fuel properties are summarized in Table 9.

Table 9. Properties of fuels used.

Fuel	Hydrogen Content (% mass)	Aromatic Content (% volume)	Sulfur Content (ppmm)
Jet A1	13.85	18.5	500
JP-5	13.52	20.1	200
ATJ Blend	14.91	8	0

The sampling system and instrumentation set-up as well as the particle losses through the sampling system for the CAAFCEB campaign remained unchanged from the previous CAAFCER campaign and are described in detail in Chapter 2.1.1 and Chapter 2.1.2.

3.1.2 Methodology to determine particle number emission index ratio

As in the CAAFCER campaign, since the CT-133 flew through aged contrails, calculating the particle number emission index (EI_N, the number of particles generated per mass of fuel burned) requires a method to account for the dilution of the plumes. Unfortunately there is no engine emissions data available in the ICAO Aircraft Engine Emissions Databank (2019)

for the Falcon 20 engines (GE CF700-2D2 model engines) and therefore the Boeing Fuel Flow Method 2 (DuBois and C. Paynter, 2006) could not be used to determine the EI_{NOx}. Thus, the ratio of particle emissions indices was calculated instead:

$$EI_{\text{Ratio}} = \frac{EI_{\text{N}_{\text{Alt}}}}{EI_{\text{N}_{\text{Jet A1}}}} = \frac{\left(\frac{N - N_{\text{bg}}}{P_{\text{CPC}} \times \left(y_{\text{NO}_x} - y_{\text{NO}_x\text{bg}}\right)}\right)_{\text{Alt}}}{\left(\frac{N - N_{\text{bg}}}{P_{\text{CPC}} \times \left(y_{\text{NO}_x} - y_{\text{NO}_x\text{bg}}\right)}\right)_{\text{Jet A1}}} \quad (29)$$

The particle number emissions index ratio of the alternate fuel (JP-5 or ATJ) to the Jet A1 fuel was determined. The EI_{NOx} was assumed to be constant for each fuel case because it has been shown that fuel type has a negligible effect on NO_x engine emissions (Corporan et al., 2011, 2007; Moore et al., 2017). This ratio would provide the relative change in particle emission number concentrations when an alternate fuel is substituted for Jet A1.

3.1.3 Uncertainty analysis

A Monte Carlo simulation was done using the bias uncertainties for the particle number, N, background particle number, N_{bg}, NO_x concentration, y_{NOx}, and the NO_x background concentration, y_{NOxbg} of Eq. 29. The uncertainty in the CPC pressure, P_{CPC}, was assumed to be negligible because the uncertainty in N was expected to be much larger. The uncertainty in N and y_{NOx} was the same as described in Chapter 2.1.5. The uncertainties in the backgrounds, N_{bg} and y_{NOxbg} were also determined using the same process described in Chapter 2.1.5. The precision uncertainty was accounted for by combining multiple segments from the same flight where possible. For each segment (or flight) a Monte Carlo simulation was performed where the top and bottom parts of Eq. 29 were calculated separately 10,000 times and were then used to calculate 10,000 ratios. Since the same instrument was used for both the alternate and Jet A1 fuel

measurements, by taking the ratio, the bias uncertainties would ideally cancel out (ie. There would be no uncertainty in the particle number, N, and NO_x concentration, y_{NOx}.). By including the uncertainties for N and y_{NOx}, a worst-case scenario is being assumed where there is some variation in the performance of the instruments during the back-to-back measurements of the exhaust plumes from the different fuels.

The method to select the segments of flight data for the analysis of the particle number emissions index ratio is the same as described in Chapter 2.1.4. Sample histograms plots for the particle and NO_x concentration and background results for one segment of the Dec 21 Jet A1 flight are shown in Figure 16. Only sample inputs for one type of fuel is shown because all fuels had similar inputs.

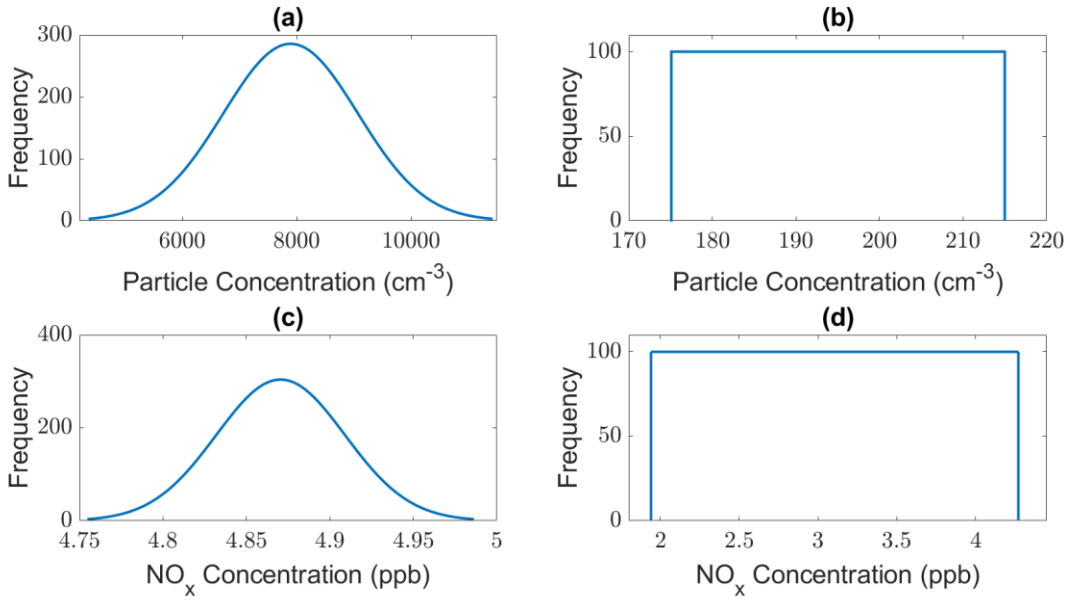

Figure 16. Sample inputs for the Monte Carlo Simulation for one segment of the Dec 21 Jet A1 flight (alternative fuels had similar inputs as well); (a) particle number concentration (TSI 3776), (b) background particle concentration (TSI 3776), (c) NOx concentration and (d) background NOx concentration.

For the Nov 20 flight, the ratio of particle emission indices between JP-5 and Jet A1 were determined. The resulting histogram plots and cumulative distribution plots for the particle emission index ratios of JP-5/Jet A1 from the 3776 CPC and 7610 CPC are shown in Figure 17. By using the cumulative distribution plots, the upper and lower limits were taken at the 95% and 5% levels respectively.

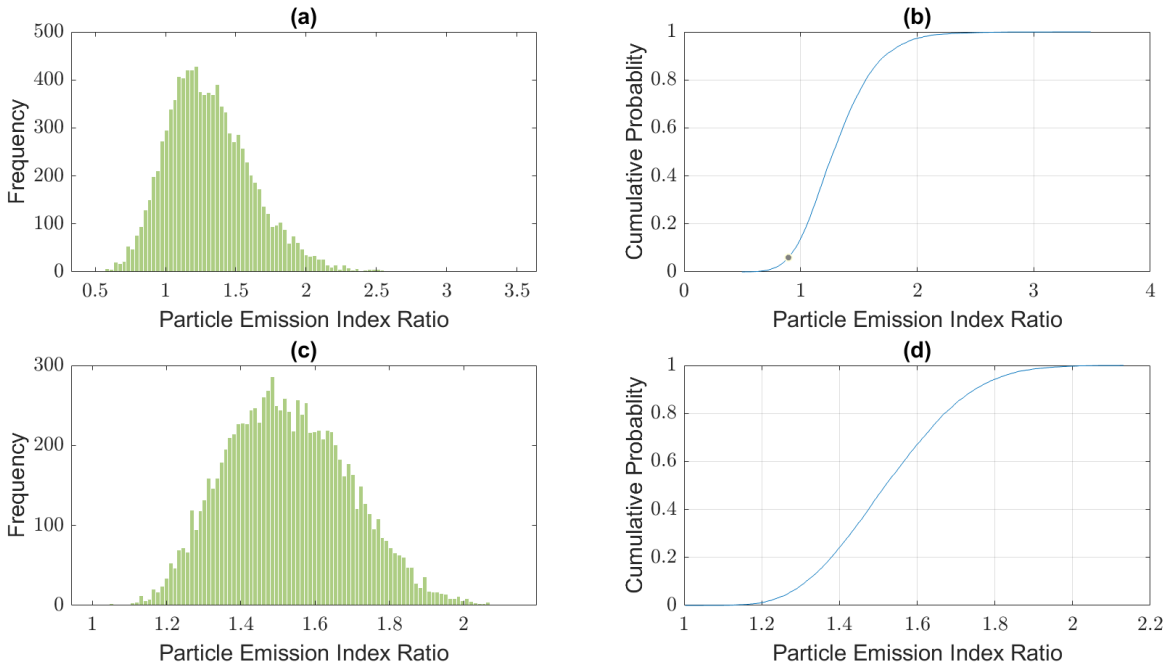

Figure 17. Monte Carlo results for Nov 20 total particle emission index ratio. (a) distribution for the TSI 3776 (b) cumulative distribution for the TSI 3776 (c) distribution for the TSI 7610 (d) cumulative distribution for the TSI 7610.

The Dec 21 flights included a total of 2 separate denuded and non-denuded segments for both fuel cases. The multimodal peaks seen in Figure 18 are a result of combining the 2 segments in each case to produce an overall distribution. The plots in Figure 17 do not have any multimodal features because it was difficult to separate the flight measurements into separate

segments due to the concentrations not fully reaching background levels in between peaks. A summary of the final results for all cases is shown in Table 10.

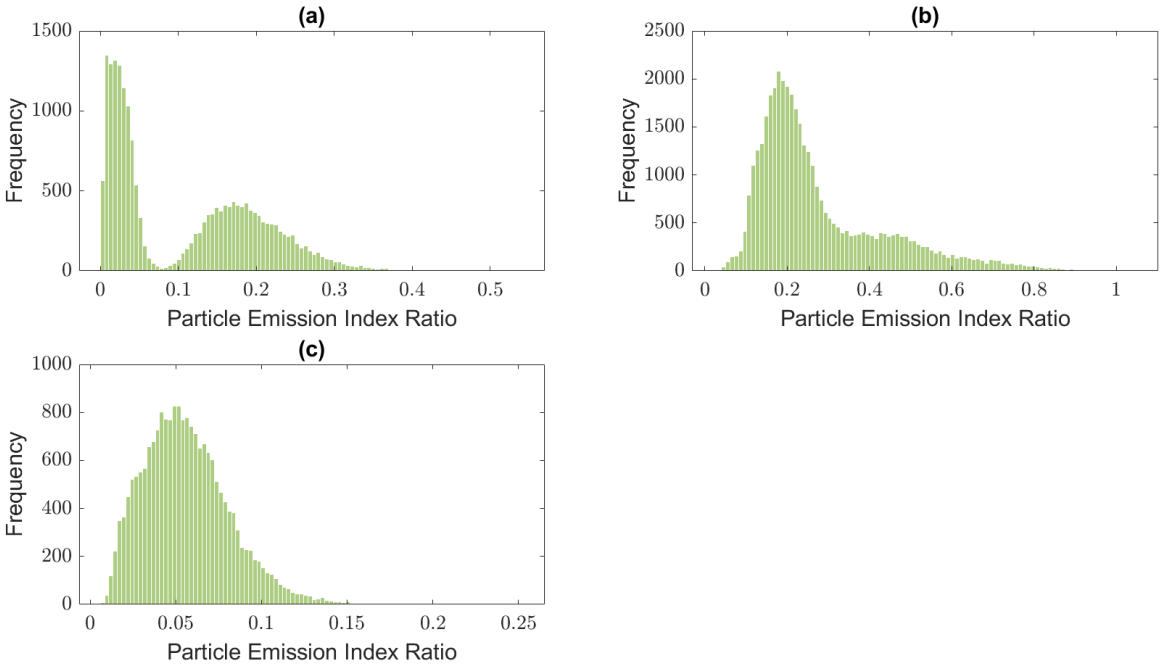

Figure 18. Monte Carlo results for Dec 21 flight particle emission index ratio between ATJ and Jet A1. (a) distribution for total particles from the TSI 3776 (b) distribution for total particles from the TSI 7610 (c) distribution for non-volatile particles from the TSI 3776.

Table 10. Summary of the final particle number emission index ratios for the CAAFCEB campaign. The particle number emission index ratios were calculated using integrals and the confidence intervals were determined from the Monte Carlo simulation.

Flight Day	Fuel Types	Particle Type	Effective Cut-Off Diameter (nm)	Particle Number Emission Index Ratio	Uncertainty Upper limit (95%)	Uncertainty Upper limit (95%)
Nov 20	JP-5/Jet A1	Total	7.7	1.29	1.87	0.88
Nov 20	JP-5/Jet A1	Total	15.4	1.52	1.82	1.26
Dec 21	ATJ/Jet A1	Total	7.7	0.09	0.27	0.01
Dec 21	ATJ/Jet A1	Total	15.4	0.33	0.62	0.11
Dec 21	ATJ/Jet A1	Non-Volatile	13.3	0.04	0.10	0.02

3.2 Results and discussion

The analysis of the two flights was completed following the procedure mentioned previously and the final results are shown in Figure 19. The results include total particle number emission indices ratios for particles with diameter d_p > 7.7 nm (for 3776 CPC) and d_p > 15.4 nm (for 7610 CPC) and non-volatile particle number emission indices ratios for particles with d_p > 13.3 nm (for 3776 CPC with catalytic denuder).

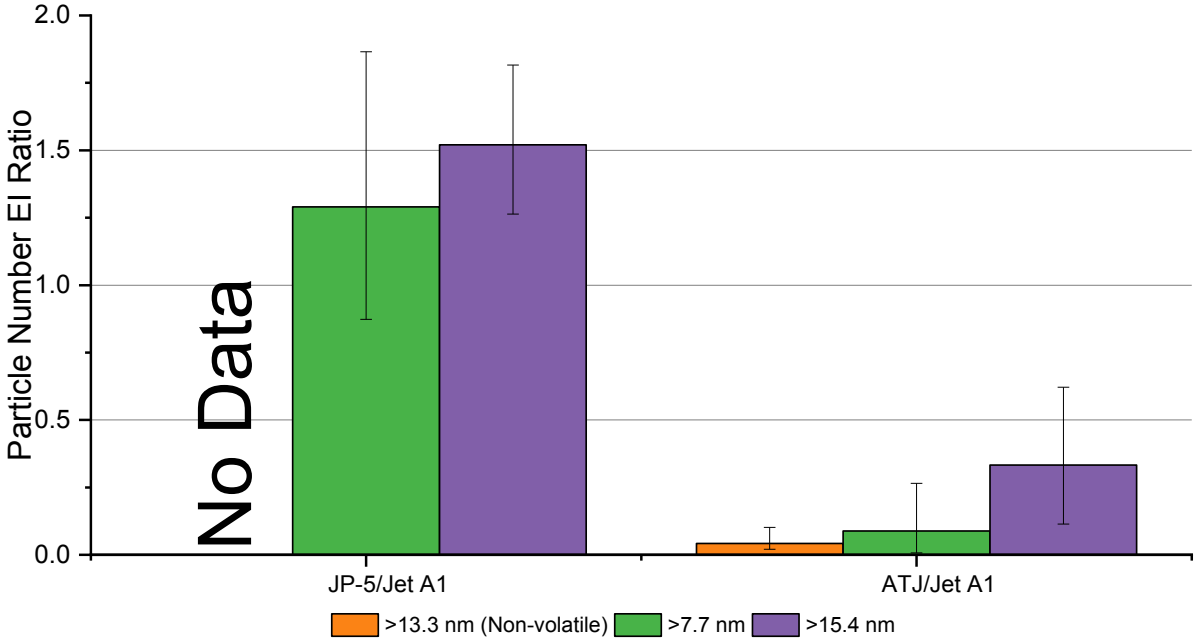

Figure 19. Particle number emission indices ratios for JP-5 and ATJ with respect to Jet A1.

From Figure 19, it can be seen that the JP-5 fuel emissions tends to have more total particles than the Jet A1 fuel. In the case for total particles larger than 7.7 nm, the JP-5 emits slightly more particles at 1.29 times that of Jet A1 but with the uncertainty taken into consideration, there may be not much of a difference. For the total particles larger than 15.4 nm case on the other hand, the JP-5 fuel produces 1.52 times more particles than Jet A1. A large difference was not expected due to both being conventional fossil-fuel derived jet fuels with similar fuel compositions as shown in Table 9. Although the JP-5 seems to emit slightly more total particles than Jet A1 but with the error bars taken into consideration, this difference may not be as big as it appears.

The ATJ fuel on the other hand showed a significant reduction in both total and non-volatile particles for all size ranges. For total particles, the ratios were 0.09 and 0.33 for particles larger than 7.7 nm and 15.4 nm respectively. The decrease in the total particle number ratios

from d_p = 15.4 nm to d_p = 7.7 nm meant that the ATJ produced fewer total particles smaller than 15.4 nm than the Jet A1. This is likely due to the ATJ fuel having near-zero fuel sulfur content (FSC) compared to Jet A1 which would result in fewer volatile particles. Volatile particles are generally found in the sub-10 nm range (Schröder et al., 2000) and it has been shown that FSC influences particle emissions (Moore et al., 2015). As shown in Table 9, the Jet A1 fuel had a FSC of 500 ppm while the ATJ fuel had a FSC of 0 ppm. This is in line with the study by Moore *et al.* that found reducing FSC from 1500 ppm to < 100 ppm resulted in a substantial decrease in particle number emissions (Moore et al., 2015). The results also further support the idea that a large change in FSC is required to have a significant effect on particle number emissions as in a separate study, Moore *et al.* found no observable effect on particle number emissions when the FSC changed from 416 ppm to 22 ppm (Moore et al., 2017).

The largest difference was seen in the non-volatile particles larger than 13.3 nm where the ratio of ATJ to Jet A1 was 0.04. The ATJ fuel produced significantly fewer non-volatile particles than the Jet A1 fuel. The reduction in non-volatile particle emissions could be a result of the differences in both the hydrogen and aromatic content. The ATJ fuel had a slightly higher hydrogen content (1.08 times higher) than the Jet A1 fuel and it has been shown that lower hydrogen content tends to produce more non-volatile particles (Corporan et al., 2011, 2007). Additionally, the aromatic content of the ATJ fuel is 0.43 times lower than the Jet A1 fuel and many studies also showed that reducing aromatic content in fuel results in a reduction of non-volatile particles (Corporan et al., 2007; DeWitt et al., 2008; Lobo et al., 2011). This is likely due to decreased aromatic content reducing precursors which contribute to the formation of soot nuclei (Corporan et al., 2007). The aromatic content in fuel can promote the growth of larger polycyclic aromatic hydrocarbons which can nucleate into soot particles (Brem et al., 2015;

DeWitt et al., 2008). Lobo et al. (2011) found that switching from Jet A1 fuel (with 18.5% vol aromatic content) to Fischer-Tropsch fuel with near zero aromatic content (<0.2% vol aromatic content) reduced particle number emissions by 52% while Corporan et al. (2007) found that switching from JP-8 fuel (15.9% vol aromatic content) to Fischer-Tropsch fuel (<0.1% vol aromatic content) led to a reduction of greater than 90% in particle number emissions. It is evident that the aromatic content of the fuel plays an important role in the production of particle emissions. Although both hydrogen and aromatic content effect particle number emissions, they are interdependent (decreasing aromatic content tends to increase the hydrogen/carbon ratio) (Lobo et al., 2011) and therefore it is difficult to credit either one as the main reason for the reduction in particles with the ATJ (Corporan et al., 2007).

CAAFCEB flight campaign is the first in-flight study to examine and compare particle number emissions from ATJ alternative fuel to conventional Jet A1 and JP-5 fuels. The results show that ATJ is a promising alternative fuel that can reduce total particle emissions by up to 91% and non-volatile particle number emissions by up to 96%. Since the current ASTM standards limits the use of biofuels to a maximum of 50% volume with conventional jet fuel, the full benefits of biofuel cannot currently be utilized. Thus, more work on fully characterizing and understanding the effects of biofuels on aircraft emissions will aid in the continued effort to update standards and technology to better utilize biofuels as an alternative fuel.

Chapter 4 Conclusion

4.1 Summary

A new particle concentration measurement system was shown and described which allows for the measurement of both total and non-volatile particles while using NO_x as a trace gas. The transport efficiency through the sampling system and the CPCs were modeled and showed that the loss of small particles can be significant enough to alter the effective cut-off diameters of the CPCs. The measurement system was used in two flight campaigns and provided additional data on particle number emissions from in-flight aircraft.

In the CAAFCER campaign three Air Canada Airbus A320 aircrafts were sampled; two burning Jet A1 fuel and one burning a 43% HEFA/Jet A1 blend. From the results, it was found that the majority of total particle numbers (~95-98% if neglecting the cut-off diameter differences) were made up of volatile particles. Despite the use of two different fuels, the results showed that there was no discernible difference between the particle number emissions. Although the use of different planes for each test meant a direct comparison would not be representative of the effect of the fuels. Additionally, the two Jet A1 flights also had slightly different fuel compositions which would explain why the particle emissions were different. The total and non-volatile particle number emission indices for this project were larger than the average particle emission indices of previous literature by a factor of 7 and 4 respectively. The average FSC for the tests in this study are about an order of magnitude higher than the average of previous studies which could help explain the total particle numbers difference. Other factors that may affect the particle number emissions include instrument cut-off diameters, the formation of contrails and contrail age. With these variables as well as fuel composition and engine models,

it is difficult to conclude the exact reason for the differences in particle number emissions found in this study.

The CAAFCEB campaign on the other hand compared JP-5 and an ATJ blend to Jet A1 fuel using the Falcon 20 research aircraft as the source of emissions. Due to the lack of publicly available emissions data for the GE CF700-2D2 engines found on the Falcon 20, the ratio of particle number emission indices was calculated instead of the particle number emission indices as was done in the CAAFCER study. The results showed that the JP-5 fuel produced slightly more total particles than the Jet A1 fuel at 1.29 times larger for d_p > 7.7 nm (for 3776 CPC) and 1.52 times larger for d_p > 15.4 nm. The fuel composition between the JP-5 and Jet A1 fuels were similar so a large difference between the particle number emissions was not expected. The ATJ fuel blend on the other hand resulted in a large reduction in both total and non-volatile particle numbers. For total particles, the ratio of emission indices for ATJ to Jet A1 were 0.09 and 0.33 for d_p > 7.7 nm and d_p > 15.4 nm respectively. This large reduction in total particles is likely due to the reduction of FSC in the Jet A1 (500 ppm) to ATJ (~0 ppm) which would reduce the number of volatile particles produced. The non-volatile particle numbers for d_p > 13.3 nm saw the largest reduction with the ratio between the ATJ and Jet A1 being 0.04. The likely reason for the reduction in non-volatile particles is the slight increase in hydrogen content of the ATJ and the aromatic content of the ATJ being half of the Jet A1 fuel. Although the ATJ showed promising results in reducing the particle number emissions, the current ASTM standards requiring biofuels to be blended to a max of 50% with conventional jet fuel limits the use of alternative biofuels to the full potential.

4.2 Future work

Although many studies have been completed (both on the ground and in flight) to measure particle number emissions from aircraft engines, it can be difficult to compare reported particle number emission indices due to the various conditions from study to study. Factors such as engine models, fuel composition, operating conditions and ambient conditions which measurements were made in have been shown to affect particle numbers. Recommendations for future work include reporting these conditions along with their corresponding particle number emission indices which would allow for better comparisons between future studies and to better identify the reasons for any differences in particle number measurements.

Throughout the two flight campaigns presented here, not every flight's data was able to be analyzed due to various instrument malfunctions. Therefore, instrumentation improvements could be made to modify the instruments to better perform in the environmental conditions found at high altitudes during flights. For example, the TSI 3776 CPC often reported errors with either inlet flowrate or aerosol flowrate which is likely due to the lower pressures found at high altitudes as well as the high speed of the aircraft. Improved flow regulation in the CPCs, could prevent these errors and allow for more accurate particle number measurements. Also, including an additional instrument to measure size distribution to be able to correct for losses and provide more detailed data on the size and number of particles would also allow for the determination of more accurate particle numbers.

References

Anderson B. E., Cofer W. R., Bagwell D. R., Barrick J. W., Hudgins C. H., Brunke K. E., 1998. Airborne observations of aircraft aerosol emissions I: Total nonvolatile particle emission indices. Geophysical Research Letters 25, 1689–1692. https://doi.org/10.1029/98GL00063

Anderson B. E., Cofer W. R., Crawford J., Gregory G. L., Vay S. A., Brunke K. E., Kondo Y., Koike M., Schlager H., Baughcum S. L., Jensen E., Zhao Yongjing, Kita Kazuyuki, 1999. An assessment of aircraft as a source of particles to the upper troposphere. Geophysical Research Letters 26, 3069–3072. https://doi.org/10.1029/1999GL900276

Anderson, B.E., Cofer, W.R., Barrick, J.D., Bagwell, D.R., Hudgins, C.H., 1998. Airborne observations of aircraft aerosol emissions II: Factors controlling volatile particle production. Geophysical Research Letters 25, 1693–1696. https://doi.org/10.1029/98GL00661

Anderson, B.E.B., 2011. Alternative Aviation Fuel Experiment (AAFEX).

ASME, 2013. PTC 19.1-2013 Test Uncertainty. The American Sociert of Mechanical Engineers (ASME), New York, NY.

ASTM D7566-19, 2019. Standard Specification for Aviation Turbine Fuel Containing Synthesized Hydrocarbons. ASTM International, West Conshohocken, PA.

ATAG, 2018. Aviation: Benefits Beyond Borders. Air Transport Action Group (ATAG), Geneva, Switzerland.

Barrett, S.R.H., Britter, R.E., Waitz, I.A., 2010. Global Mortality Attributable to Aircraft Cruise Emissions. Environ. Sci. Technol. 44, 7736–7742. https://doi.org/10.1021/es101325r

Bendtsen, K.M., Brostrøm, A., Koivisto, A.J., Koponen, I., Berthing, T., Bertram, N., Kling, K.I., Dal Maso, M., Kangasniemi, O., Poikkimäki, M., Loeschner, K., Clausen, P.A., Wolff, H., Jensen, K.A., Saber, A.T., Vogel, U., 2019. Airport emission particles: exposure characterization and toxicity following intratracheal instillation in mice. Particle and Fibre Toxicology 16, 23. https://doi.org/10.1186/s12989-019-0305-5

Beyersdorf, A.J., Timko, M.T., Ziemba, L.D., Bulzan, D., Corporan, E., Herndon, S.C., Howard, R., Miake-Lye, R., Thornhill, K.L., Winstead, E., Wey, C., Yu, Z., Anderson, B.E., 2014. Reductions in aircraft particulate emissions due to the use of Fischer–Tropsch fuels. Atmos. Chem. Phys. 14, 11–23. https://doi.org/10.5194/acp-14-11-2014

Brem, B.T., Durdina, L., Siegerist, F., Beyerle, P., Bruderer, K., Rindlisbacher, T., Rocci-Denis, S., Andac, M.G., Zelina, J., Penanhoat, O., Wang, J., 2015. Effects of Fuel Aromatic Content on Nonvolatile Particulate Emissions of an In-Production Aircraft Gas Turbine. Environ. Sci. Technol. 49, 13149–13157. https://doi.org/10.1021/acs.est.5b04167

Brock, C.A., Schröder, F., Kärcher, B., Petzold, A., Busen, R., Fiebig, M., 2000. Ultrafine particle size distributions measured in aircraft exhaust plumes. Journal of Geophysical Research: Atmospheres 105, 26555–26567. https://doi.org/10.1029/2000JD900360

Catalytic Stripper Manual, 2016.

Chan, T.W., Chishty, W.A., Canteenwalla, P., Buote, D., Davison, C.R., 2015. Characterization of Emissions From the Use of Alternative Aviation Fuels. Journal of Engineering for Gas Turbines and Power 138. https://doi.org/10.1115/1.4031226

Cofer, W.R., Anderson, B.E., Winstead, E.L., Bagwell, D.R., 1998. Calibration and demonstration of a condensation nuclei counting system for airborne measurements of aircraft exhausted particles. Atmospheric Environment 32, 169–177. https://doi.org/10.1016/S1352-2310(97)00318-X

Corporan, E., DeWitt, M.J., Belovich, V., Pawlik, R., Lynch, A.C., Gord, J.R., Meyer, T.R., 2007. Emissions Characteristics of a Turbine Engine and Research Combustor Burning a Fischer−Tropsch Jet Fuel. Energy Fuels 21, 2615–2626. https://doi.org/10.1021/ef070015j

Corporan, E., Edwards, T., Shafer, L., DeWitt, M.J., Klingshirn, C., Zabarnick, S., West, Z., Striebich, R., Graham, J., Klein, J., 2011. Chemical, Thermal Stability, Seal Swell, and Emissions Studies of Alternative Jet Fuels. Energy Fuels 25, 955–966. https://doi.org/10.1021/ef101520v

DeWitt, M.J., Corporan, E., Graham, J., Minus, D., 2008. Effects of Aromatic Type and Concentration in Fischer−Tropsch Fuel on Emissions Production and Material Compatibility. Energy Fuels 22, 2411–2418. https://doi.org/10.1021/ef8001179

DuBois, D., C. Paynter, G., 2006. "Fuel Flow Method2" for Estimating Aircraft Emissions. https://doi.org/10.4271/2006-01-1987

Febvre, G., Gayet, J.-F., Minikin, A., Schlager, H., Shcherbakov, V., Jourdan, O., Busen, R., Fiebig, M., Kärcher, B., Schumann, U., 2009. On optical and microphysical characteristics of contrails and cirrus. Journal of Geophysical Research: Atmospheres 114. https://doi.org/10.1029/2008JD010184

Gutiérrez-Antonio, C., Gómez-Castro, F.I., de Lira-Flores, J.A., Hernández, S., 2017. A review on the production processes of renewable jet fuel. Renewable and Sustainable Energy Reviews 79, 709–729. https://doi.org/10.1016/j.rser.2017.05.108

He, T., Wang, D., Qu, Y., 2018. 5.06 - Land Surface Albedo, in: Liang, S. (Ed.), Comprehensive Remote Sensing. Elsevier, Oxford, pp. 140–162. https://doi.org/10.1016/B978-0-12-409548-9.10370-7

ICAO, 2017. ANNEX 16 - ENVIRONMENTAL PROTECTION VOLUME 2 - AIRCRAFT ENGINE EMISSIONS, 4th ed. International Civil Aviation Organization, Montréal, Quebec, Canada.

ICAO, 2016. ICAO Environmental Report 2016. International Civil Aviation Organization (ICAO), Quebec, Canada.

ICAO, 1993. MANUAL OF THE ICAO STANDARD ATMOSPHERE extended to 80 kilometres (262 500 feet), 3rd ed. International Civil Aviation Organization, Montréal, Québec, Canada.

ICAO Aircraft Engine Emissions Databank, 2019.

ISO 5878, 1990. Reference Atmospheres for Aerospace Use. The International Organization for Standardization (ISO).

Jonsdottir, H.R., Delaval, M., Leni, Z., Keller, A., Brem, B.T., Siegerist, F., Schönenberger, D., Durdina, L., Elser, M., Burtscher, H., Liati, A., Geiser, M., 2019. Non-volatile particle emissions from aircraft turbine engines at ground-idle induce oxidative stress in bronchial cells. Communications Biology 2, 90. https://doi.org/10.1038/s42003-019-0332-7

Kandaramath Hari, T., Yaakob, Z., Binitha, N.N., 2015. Aviation biofuel from renewable resources: Routes, opportunities and challenges. Renewable and Sustainable Energy Reviews 42, 1234–1244. https://doi.org/10.1016/j.rser.2014.10.095

Kärcher, B., Busen, R., Petzold, A., Schröder, F.P., Schumann, U., Jensen, E.J., 1998. Physicochemistry of aircraft-generated liquid aerosols, soot, and ice particles: 2. Comparison with observations and sensitivity studies. Journal of Geophysical Research: Atmospheres 103, 17129–17147. https://doi.org/10.1029/98JD01045

Kulkarni, P., Baron, P.A., Willeke, K. (Eds.), 2011. Aerosol measurement principles, techniques, and applications, 3rd ed. ed. Wiley, Hoboken, N.J.

Lee, D.S., 2009. Aviation and Climate Change: The Science, in: Gössling, S., Upham, P. (Eds.), Climate Change and Aviation: Issues, Challenges and Solutions. Earthscan, London.

Lobo, P., Hagen, D.E., Whitefield, P.D., 2011. Comparison of PM Emissions from a Commercial Jet Engine Burning Conventional, Biomass, and Fischer–Tropsch Fuels. Environ. Sci. Technol. 45, 10744–10749. https://doi.org/10.1021/es201902e

Lois, E., Keating, E.L., Gupta, A.K., 2003. Fuels, in: Meyers, R.A. (Ed.), Encyclopedia of Physical Science and Technology (Third Edition). Academic Press, New York, pp. 275–314. https://doi.org/10.1016/B0-12-227410-5/00268-4

Lopes, M., Russo, A., Monjardino, J., Gouveia, C., Ferreira, F., 2019. Monitoring of ultrafine particles in the surrounding urban area of a civilian airport. Atmospheric Pollution Research 10, 1454–1463. https://doi.org/10.1016/j.apr.2019.04.002

Lukachko, S.P., Waitz, I.A., 1997. Effects of Engine Aging on Aircraft NOx Emissions V001T01A011. https://doi.org/10.1115/97-GT-386

Moore, R.H., Shook, M., Beyersdorf, A., Corr, C., Herndon, S., Knighton, W.B., Miake-Lye, R., Thornhill, K.L., Winstead, E.L., Yu, Z., Ziemba, L.D., Anderson, B.E., 2015. Influence of Jet Fuel Composition on Aircraft Engine Emissions: A Synthesis of Aerosol Emissions Data from the NASA APEX, AAFEX, and ACCESS Missions. Energy Fuels 29, 2591–2600. https://doi.org/10.1021/ef502618w

Moore, R.H., Thornhill, K.L., Weinzierl, B., Sauer, D., D'Ascoli, E., Kim, J., Lichtenstern, M., Scheibe, M., Beaton, B., Beyersdorf, A.J., Barrick, J., Bulzan, D., Corr, C.A., Crosbie, E., Jurkat, T., Martin, R., Riddick, D., Shook, M., Slover, G., Voigt, C., White, R., Winstead, E., Yasky, R., Ziemba, L.D., Brown, A., Schlager, H., Anderson, B.E., 2017. Biofuel blending reduces particle emissions from aircraft engines at cruise conditions. Nature 543, 411. https://doi.org/10.1038/nature21420

Pechstein, J., Neuling, U., Gebauer, J., Kaltschmitt, M., 2018. Alcohol-to-Jet (AtJ), in: Kaltschmitt, M., Neuling, U. (Eds.), Biokerosene: Status and Prospects. Springer Berlin Heidelberg, Berlin, Heidelberg, pp. 543–574. https://doi.org/10.1007/978-3-662-53065-8_21

Peck, J., Oluwole, O.O., Wong, H.-W., Miake-Lye, R.C., 2013. An algorithm to estimate aircraft cruise black carbon emissions for use in developing a cruise emissions inventory. Journal of the Air & Waste Management Association 63, 367–375. https://doi.org/10.1080/10962247.2012.751467

Petzold, A., Busen, R., Schröder, F.P., Baumann, R., Kuhn, M., Ström, J., Hagen, D.E., Whitefield, P.D., Baumgardner, D., Arnold, F., Borrmann, S., Schumann, U., 1997. Near-field measurements on contrail properties from fuels with different sulfur content. Journal of Geophysical Research: Atmospheres 102, 29867–29880. https://doi.org/10.1029/97JD02209

Petzold, A., Döpelheuer, A., Brock, C.A., Schröder, F., 1999. In situ observations and model calculations of black carbon emission by aircraft at cruise altitude. Journal of

Geophysical Research: Atmospheres 104, 22171–22181. https://doi.org/10.1029/1999JD900460
Petzold, A., Ogren, J.A., Fiebig, M., Laj, P., Li, S.-M., Baltensperger, U., Holzer-Popp, T., Kinne, S., Pappalardo, G., Sugimoto, N., Wehrli, C., Wiedensohler, A., Zhang, X.-Y., 2013. Recommendations for reporting "black carbon" measurements. Atmospheric Chemistry and Physics 13, 8365–8379. https://doi.org/10.5194/acp-13-8365-2013
Pui, D.Y.H., Romay-Novas, F., Liu, B.Y.H., 1987. Experimental Study of Particle Deposition in Bends of Circular Cross Section. Aerosol Science and Technology 7, 301–315. https://doi.org/10.1080/02786828708959166
Pulselli, F.M., Marchi, M., 2015. Global Warming Potential and the Net Carbon Balance☆, in: Reference Module in Earth Systems and Environmental Sciences. Elsevier. https://doi.org/10.1016/B978-0-12-409548-9.09526-9
SAE, 2018. Procedure for the Continuous Sampling and Measurement of Non-Volatile Particulate Matter Emissions from Aircraft Turbine Engines, SAE Standard ARP6320. https://doi.org/10.4271/ARP6320
SAE, 2006. Regulation No 83 of the Economic Commission for Europe of the United Nations (UN/ECE) – Uniform provisions concerning the approval of vehicles with regard to the emission of pollutants according to engine fuel requirements. Official Journal of the European Union 49, 233–495.
SAE, 1970. Aircraft Gas Turbine Engine Exhaust Smoke Measurement, SAE Standard ARP1179. https://doi.org/10.4271/ARP1179D
Schripp, T., Herrmann, F., Oßwald, P., Köhler, M., Zschocke, A., Weigelt, D., Mroch, M., Werner-Spatz, C., 2019. Particle emissions of two unblended alternative jet fuels in a full scale jet engine. Fuel 256, 115903. https://doi.org/10.1016/j.fuel.2019.115903
Schröder, F., Brock, C.A., Baumann, R., Petzold, A., Busen, R., Schulte, P., Fiebig, M., 2000. In situ studies on volatile jet exhaust particle emissions: Impact of fuel sulfur content and environmental conditions on nuclei mode aerosols. Journal of Geophysical Research: Atmospheres 105, 19941–19954. https://doi.org/10.1029/2000JD900112
Schröder, F.P., Kärcher, B., Petzold, A., Baumann, R., Busen, R., Hoell, C., Schumann, U., 1998. Ultrafine aerosol particles in aircraft plumes: In situ observations. Geophysical Research Letters 25, 2789–2792. https://doi.org/10.1029/98GL02078
Schulte P., Schlager H., Ziereis H., Schumann U., Baughcum S. L., Deidewig F., 1997. NO x emission indices of subsonic long-range jet aircraft at cruise altitude: In situ measurements and predictions. Journal of Geophysical Research: Atmospheres 102, 21431–21442. https://doi.org/10.1029/97JD01526
Schumann, U., Arnold, F., Busen, R., Curtius, J., Kärcher, B., Kiendler, A., Petzold, A., Schlager, H., Schröder, F., Wohlfrom, K.-H., 2002. Influence of fuel sulfur on the composition of aircraft exhaust plumes: The experiments SULFUR 1–7. Journal of Geophysical Research: Atmospheres 107, AAC 2-1-AAC 2-27. https://doi.org/10.1029/2001JD000813
Schumann, U., Ström, J., Busen, R., Baumann, R., Gierens, K., Krautstrunk, M., Schröder, F.P., Stingl, J., 1996. In situ observations of particles in jet aircraft exhausts and contrails for different sulfur-containing fuels. Journal of Geophysical Research: Atmospheres 101, 6853–6869. https://doi.org/10.1029/95JD03405

Stacey, B., 2019. Measurement of ultrafine particles at airports: A review. Atmospheric Environment 198, 463–477. https://doi.org/10.1016/j.atmosenv.2018.10.041
Takegawa, N., Iida, K., Sakurai, H., 2017. Modification and laboratory evaluation of a TSI ultrafine condensation particle counter (Model 3776) for airborne measurements. Aerosol Science and Technology 51, 235–245. https://doi.org/10.1080/02786826.2016.1261990
Terzano, C., Di Stefano, D., Conti, V., Graziani, E., Petroianni, A., 2010. Air pollution ultrafine particles: toxicity beyond the lung. Eur Rev Med Pharmacol Sci 14, 809–821.
Timko, M.T., Yu, Z., Onasch, T.B., Wong, H.-W., Miake-Lye, R.C., Beyersdorf, A.J., Anderson, B.E., Thornhill, K.L., Winstead, E.L., Corporan, E., DeWitt, M.J., Klingshirn, C.D., Wey, C., Tacina, K., Liscinsky, D.S., Howard, R., Bhargava, A., 2010. Particulate Emissions of Gas Turbine Engine Combustion of a Fischer−Tropsch Synthetic Fuel. Energy Fuels 24, 5883–5896. https://doi.org/10.1021/ef100727t
TSI, 2011. Model 3776 Ultrafine Condensation Particle Counter Operation and Service Manual.
US Department of Commerce, N., n.d. NOAA/ESRL Global Monitoring Division - THE NOAA ANNUAL GREENHOUSE GAS INDEX (AGGI) [WWW Document]. URL https://www.esrl.noaa.gov/gmd/aggi/aggi.html (accessed 1.9.20).
Vander Wal, R.L., Bryg, V.M., Huang, C.-H., 2014. Aircraft engine particulate matter: Macro-micro- and nanostructure by HRTEM and chemistry by XPS. Combustion and Flame 161, 602–611. https://doi.org/10.1016/j.combustflame.2013.09.003
Vozka, P., Šimáček, P., Kilaz, G., 2018. Impact of HEFA Feedstocks on Fuel Composition and Properties in Blends with Jet A. Energy Fuels 32, 11595–11606. https://doi.org/10.1021/acs.energyfuels.8b02787
Wang, X., Horn, H.-G., 2008. FLOW RATE CORRECTION FOR THE MODEL 3790 ENGINE EXHAUST CONDENSATION PARTICLE COUNTER (EECPC).
WHO, 2018. Ambient (outdoor) air quality and health [WWW Document]. World Health Organization. URL https://www.who.int/en/news-room/fact-sheets/detail/ambient-(outdoor)-air-quality-and-health (accessed 2.13.19).
Willeke, K., 1976. Temperature dependence of particle slip in a gaseous medium. Journal of Aerosol Science 7, 381–387. https://doi.org/10.1016/0021-8502(76)90024-0
Wise, M., Muratori, M., Kyle, P., 2017. Biojet fuels and emissions mitigation in aviation: An integrated assessment modeling analysis. Transportation Research Part D: Transport and Environment 52, Part A, 244–253. https://doi.org/10.1016/j.trd.2017.03.006
Zhang, X., Chen, X., Wang, J., 2019. A number-based inventory of size-resolved black carbon particle emissions by global civil aviation. Nature Communications 10, 534. https://doi.org/10.1038/s41467-019-08491-9
Zhang, Z., Liu, B.Y.H., 1991. Performance of TSI 3760 Condensation Nuclei Counter at Reduced Pressures and Flow Rates. Aerosol Science and Technology 15, 228–238. https://doi.org/10.1080/02786829108959530